Analog Pre-distortion Circuit for Simultaneous Suppression of Third and Fifth Order Intermodulation Distortion in Broadband Radio-over-Fiber Systems

Shuvasish Saha

A Thesis

in

The Department

of

Electrical and Computer Engineering

Presented in Partial Fulfillment of the Requirements

For the Degree of Master of Applied Science at

Concordia University

Montreal, Quebec, Canada

September, 2016

CONCORDIA UNIVERSITY
SCHOOL OF GRADUATE STUDIES

This is to certify that the thesis prepared

By: Shuvasish Saha

Entitled: "Analog Pre-distortion Circuit for Simultaneous Suppression of Third and Fifth Order Intermodulation Distortion in Broadband Radio-over-Fiber Systems"

and submitted in partial fulfillment of the requirements for the degree of

Master of Applied Science

Complies with the regulations of this University and meets the accepted standards with respect to originality and quality.

Signed by the final examining committee:

_____ Chair
Dr. R. Raut

_____ Examiner, External
Dr. Jia Yuan Yu (CIISE) To the Program

_____ Examiner
Dr. G. Cowen

_____ Supervisor
Dr. X. Zhang

Approved by: _____
Dr. W. E. Lynch, Chair
Department of Electrical and Computer Engineering

_____20_____

_____
Dr. Amir Asif, Dean
Faculty of Engineering and Computer Science

ABSTRACT

Analog Pre-distortion Circuit for Simultaneous Suppression of Third and Fifth Order Intermodulation Distortion in Broadband Radio-over-Fiber Systems

Shuvasish Saha

Rapid advance in wireless technologies coupled with the exponential increase in use of high bandwidth devices and applications have made it necessary to develop high capacity wireless transmission networks. Design of robust and cost-effective wireless signal transmission systems has become of paramount importance to keep up with the breakneck pace of wireless access demand, especially keeping in mind the future of massive multiple-input and multiple-output (MIMO) wireless. Radio-over-Fiber (RoF) transmission systems are at the forefront of the research topics being investigated right now as a possible solution to keep up with this exploding demand for wireless network access.

Based on optical subcarrier modulation, RoF transmission systems combine the use of both optical fiber and radio transmission. Optical fibers are low cost. They are lightweight and suffer from low loss. They provide extremely high capacity and immunity from electromagnetic interference. Radio transmission over fiber makes it easy to assemble Remote Radio Units (RRUs) at antenna towers. However, RoF is an analog optical transmission system and it is susceptible to non-linear distortions caused by all the inline functional optical and electrical components. In case of front-haul RoF transmission systems of wireless access networks, two key specific functions: RF power amplification and optical subcarrier modulation, are the main contributors to the production of non-linear distortions. Non-linear distortions consist of harmonic distortions (HDs) and intermodulation distortions (IMDs). It is essential to suppress these distortions because they can introduce crosstalk if they fall in the passband of RF signals.

In this thesis, the use of analog pre-distortion circuit (PDC) is investigated as a linearization technique for the purpose of suppressing non-linear distortions, especially the third order intermodulation distortion (IMD3) and the fifth order intermodulation distortion (IMD5) simultaneously. An analog pre-distortion circuit (PDC) is designed and fabricated based on the

transmission characteristics of a modulator integrated distributed feed-back (DFB) laser (EML). The PDC is low cost, compact and has broad operational bandwidth. It is designed to operate in the bandwidth up to 6 GHz, using two beam-lead silicone Schottky diodes as predistorter. The linearization by this PDC is verified in EML modulated RoF transmission system. First, by using the EML modulated RoF, Spurious Free Dynamic Range (SFDR) improvement of over 11 dB is achieved related to IMD3 and over 3 dB related to IMD5 for the entire bandwidth. Similarly, the SFDR improved by more than 6 dB related to IMD3 and by more than 4 dB related to IMD5 for another EAM modulated RoF throughout the entire bandwidth. When Wi-Fi signals at 2.4 GHz and 5 GHz were transmitted through the EML modulated RoF, error vector magnitude (EVM) was improved by 1.3 dB at 2.4 GHz and by 1.55 dB at 5 GHz for back-to-back (BTB) transmission. For 10 km single mode fiber (SMF) transmission, EVM improved by 1.07 dB at 2.4 GHz and by 1.03 dB at 5 GHz. For the EAM modulated RoF, EVM was improved by 2.76 dB at 2.4 GHz and by 1.45 dB at 5 GHz for BTB transmission. For 10 km SMF transmission, EVM was improved by 2.08 dB at 2.4 GHz and by 1.44 dB at 5 GHz. Moreover, Wi-Fi signals were generated at a RF carrier of 2-5 GHz and EVM improvements were recorded. For the EML modulated RoF, EVM improvement was more than 1.4 dB for BTB transmission and more than 1 dB for 10 km SMF transmission. For the EAM modulated RoF, EVM improvement was more than 1.4 dB for both BTB and 10 km SMF transmission.

Acknowledgements

I would like to express my sincere gratitude to Professor John X. Zhang for his continuous advice, help and support for me to finish my thesis. Without his insights, it would not be possible to finish this work.

I would also like to express my appreciation to my colleagues Dr. Ran Zhu and Hakim Mellah for their continuous help and advice during the long circuit design and experimental verification processes.

I would also like to thank Dr. Ahmed A Kishk and Vincent Mooney-Chopin for providing me access to their lab and to let me use their Network Analyzer for the s-parameter measurements of my fabricated circuit.

And also I would like to thank Mr. Traian Antonescu and Mr. Maxime Thibault with Poly-Grames Research Center, Centre de Recherche en Électronique Radio fréquence (CREER) for their technical assistance and suggestions in PCB fabrication of the prototype circuit.

I am very grateful to my parents: Subrata Saha and Rita Saha for their endless love, understanding and support.

Last but not the least I would like to say a very big thanks to my wife Marzana Mahi Syeda for her unconditional love and support during my endless hours of work in the lab and for encouraging me through every thick and thin to accomplish this milestone in my life.

Table of Contents

List of Figures

List of Tables

List of Acronyms

ACP	Adjacent Channel Power
ADC	Analog-to-Digital Converter
ADS	Advanced Design Systems
AM-AM	Amplitude-to-Amplitude
ATT	Attenuator
AWG	Arbitrary Waveform Generator
BER	Bit Error Rate
BTB	Back-to-Back
CD	Chromatic Dispersion
CPU	Central Processing Unit
CW	Continuous Wave
DAC	Digital-to-Analog Converter
DC	Direct Current
DCF	Dispersion Compensated Fiber
DFB	Direct Feedback
DPC	Digital Post-Compensation
DPD	Digital Pre-distortion
DSB	Double Sideband
DSO	Digital Storage Oscilloscope
DSP	Digital Signal Processing
EAM	Electro-Absorption Modulator

EML	Electro-Absorption Modulated Laser
E/O	Electrical to Optical
EVM	Error Vector Magnitude
FWM	Four-Wave Mixing
HD	Harmonic Distortion
HD2	2nd Order Harmonic Distortion
HD3	3rd Order Harmonic Distortion
IMD	Intermodulation Distortion
IMD3	3rd Order Intermodulation Distortion
IMD5	5th Order Intermodulation Distortion
IP	Intercept Point
LD	Laser Diode
LNA	Low Noise Amplifier
MB-OFDM	Multiband Orthogonal Frequency Division Multiplexing
MIMO	Multiple-Input and Multiple-Output
MMF	Multi Mode Fiber
MP	Mixed-Polarization
MZM	Mach-Zehnder Modulator
NF	Noise Figure
O/E	Optical to Electrical
OFDM	Orthogonal Frequency-Division Multiplexing
ORx	Optical Receiver

OTx	Optical Transmitter
PA	Power Amplifier
PC	Polarization Controller
PD	Photodetector
PDC	Pre-distortion Circuit
QAM	Quadrature Amplitude Modulation
RBW	Resolution Bandwidth of Spectrum Analyser
RF	Radio Frequency
RoF	Radio-over-Fiber
RRU	Remote Radio Unit
SA	Spectrum Analyzer
SFDR	Spurious Free Dynamic Range
SMF	Single Mode Fiber
SNR	Signal-to-Noise Ratio
SOA	Semiconductor Optical Amplifier
SSB	Single Sideband
TE	Transverse Electric
TIA	Transimpedance Amplifier
TM	Transverse Magnetic
UWB	Ultra Wideband
VBW	Video Bandwidth of Spectrum Analyser
VNA	Vector Network Analyzer

WDM	Wavelength Division Multiplexing

List of Symbols

a_n	n^{th} order coefficient of the PDC
b_n	n^{th} order coefficient of the RoF system
B_v	Reverse Breakdown Voltage of Diode
β	Phase Shift
C_{jo}	Zero-bias Junction Capacitance of Diode
E_G	Activation Energy
f	Frequency
f_c	Optical Carrier
f_{RF}	RF Carrier
G	Non-linear Conductance
I_{BV}	Reverse Breakdown Current of Diode
I_d	DC current through Diode
I_S	Saturation Current of Diode
K	Boltzmann's Constant
M	Junction Grading Coefficient
η	Ideality Factor
N	Emission coefficient
P_B	Area Junction Contact Potential
p_i	Coefficient of curve fitting polynomial

P_T	Saturation Current Temperature Exponent
q	Electron Charge
R_b	Contact Resistance of Diode
R_S	Parasitic Resistance of Diode
R_{Ser}	Series Resistance
τ	Time delay
RF_{IN}	Input RF Power
RF_{Out}	Output RF Power
S_{11}	Input port voltage reflection coefficient
S_{21}	Forward Voltage Gain
t	Time
T	Absolute Temperature
V	Reversed bias voltage
V_b	Voltage applied to Junction of Schottky Barrier
V_o	Magnitude of applied voltage
V_{bias}	Bias voltage
V_{DC}	DC bias voltage
V_i	Input voltage
V_o	Output voltage
V_{RF}	RF signal voltage
V_T	Threshold Voltage of Diode

$v(t)$	AC Voltage applied to Junction of Schottky Barrier
λ	Wavelength
$\lambda/4$	Quarter wave
ω	Angular frequency
ω_{RF}	Angular frequency of the RF signal
Z_{Load}	Load Impedance
Z_s	Source Impedance

Chapter 1 Introduction

1.1 Radio-over-Fiber Transmission Systems

Radio-over-Fiber transmission systems have come back to prominence as a major research topic after lying dormant for two decades when it was first introduced and demonstrated by A J Cooper [1]. This is due to the fact that wireless enabled devices had an explosion in usage over the last decade. More and more devices and applications are being rolled out continuously which are putting a huge strain on the existing methods of wireless network service delivery. Optical components have become cheaper over the last decade and frankly, there was no need about fifteen years ago to justify huge investment in wireless transmission systems because there was not enough demand for it. Today, however, the picture is drastically different.

Traditional wireless access networks consist of back-haul and front-haul transmission systems as shown in Figure 1-1.

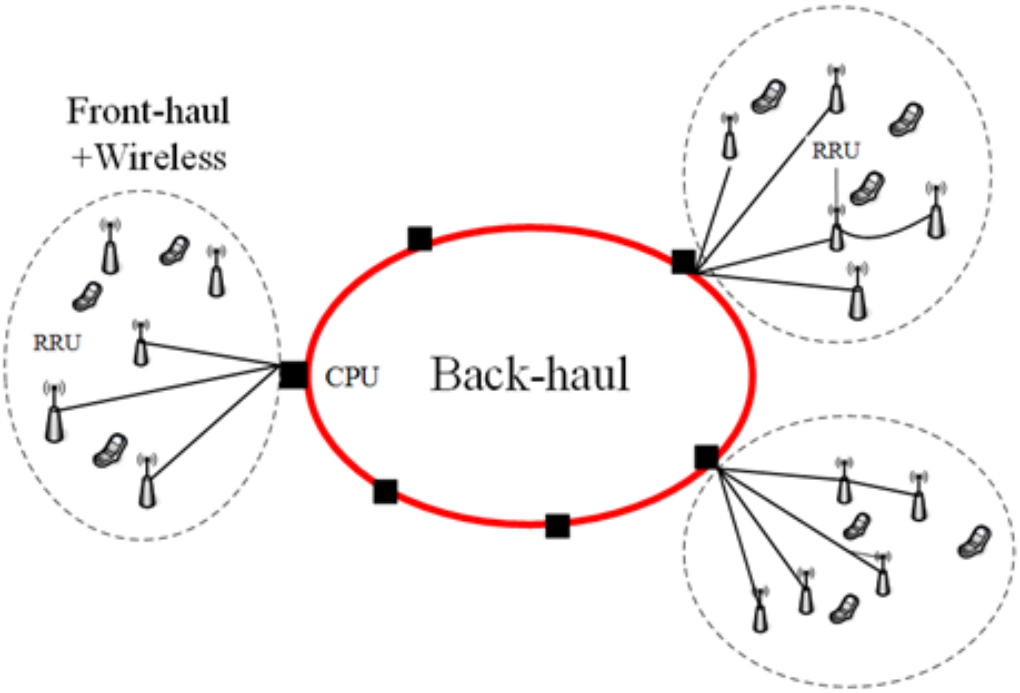

Figure 1-1: Wireless access network infrastructure with front-haul and back-haul transmission systems [2]

The back-haul networks typically use high capacity digital fiber systems to transmit baseband signals. In the front-haul networks, traditional techniques like narrow band analog radio frequency (RF) transmission over microwave coaxial cables and digital fiber transmissions are used to distribute wireless signals to antenna towers. The main drawbacks of using microwave coaxial cables are that they are too costly and bulky. They suffer from high attenuation when high frequency RF signals are transmitted through them. Optical fibers offer a remarkable amount of advantages over the use of coaxial cables. First of all, optical fibers are very lightweight and very cheap. Its main features are broad bandwidth, low loss and immunity from electromagnetic interference. In case of digital fiber transmissions, the main drawback comes from the complexity of constructing Remote Radio Units (RRUs) because digital to/from analog signal processing is required. Radio-over-Fiber (RoF) transmission systems offer a lots of advantages over these traditional methods [2].

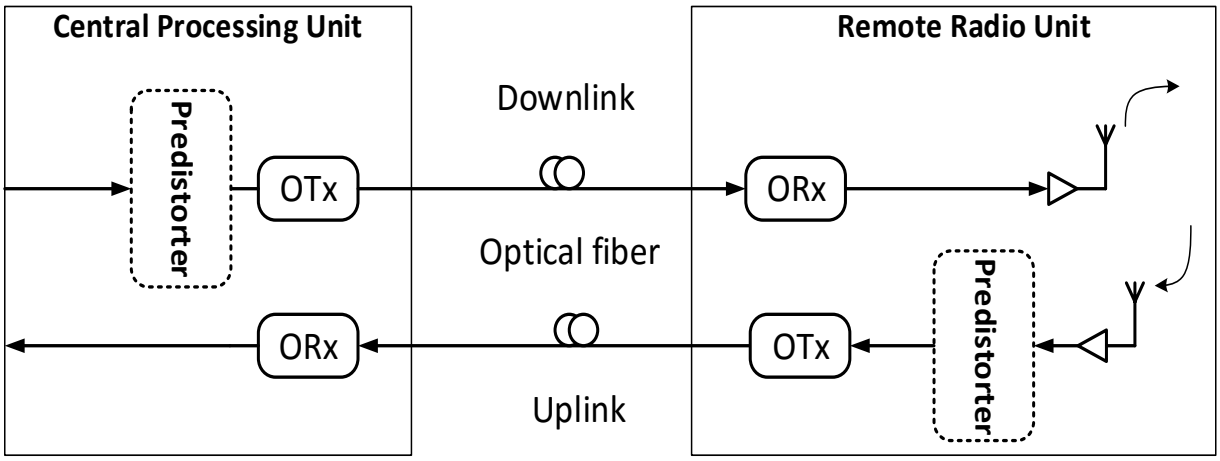

Figure 1-2: Basic configuration of RoF transmission systems

Figure 1-2 shows the basic configuration of a RoF transmission system. It consists of Central Processing Unit (CPU) and Remote Radio Unit (RRU) and combines the advantages provided by optical fiber and wireless access. The direction of transmission from the CPU to the RRU is known as the Downlink and the opposite transmission direction is known as the Uplink. In the Downlink, RF signals are generated and go through up-conversion inside the CPU before being transmitted through the optical fiber to the RRU. The optical transmitter (OTx) has an optical modulator which modulates optical carrier with RF signals. The transmitter can be a laser diode

(LD) or a laser plus an external modulator. Modulation using laser is called Direct modulation whereas modulation using laser plus an external modulator is called External modulation. External modulators like Electro-absorption modulator (EAM) or Mach-Zehnder modulator (MZM) are especially used to achieve higher modulation bandwidth. The modulated signals in the OTx are then transmitted through the optical fiber to the Optical receiver (ORx) in the RRU. For the optical fiber, Single mode fiber (SMF) or Multi-mode fiber (MMF) can be used. ORx usually consists of a Photodiode (PD) which demodulates the optical signal back to RF signal. The demodulated signal is amplified before being fed to an antenna which is then distributed to the users. The ORx, amplifier and the antenna are part of the RRU. Similarly, in the Uplink, the RF signals received by the antennas are amplified and fed into the OTx in the RRU which modulate the signals. The signals are then sent through the optical fiber to the ORx in the CPU where they are demodulated to RF signals and down-converted and processed [3]-[4]. In both the CPU and the RRU, signals are put through a predistorter initially before being fed into the OTx. This is done to counter the non-linearities produced by the modulators in the OTx.

There are several advantages of using RoF transmission systems. Firstly, the use of optical fibers instead of microwave coaxial cables between CPU and RRU provides low loss for long distance transmissions and broad bandwidth. Single Mode Fiber (SMF) is preferable to Multi-mode Fiber (MMF) for this purpose because MMF can induce modal dispersion. All the complicated and power consuming tasks like up/down conversion and analog-to-digital/digital-to-analog converters (ADCs/DACs), frequency multiplexing and signal processing can be performed at the CPU. These makes the assembly, deployment and maintaince of RRUs very easy. The RRUs are only limited to using OTx, ORx, amplifier and antenna which consumes less power and are less complicated systems. Moreover, a single CPU is capable of communicating with multiple RRUs. This is particularly helpful because high number of RRUs need to be deployed to carry the load of very high wireless access demand.

However, as with all communication systems, RoF transmission systems are not perfect. RoF systems involve analog modulation and detection of light which introduces the possibility of encountering signal noise and non-linear distortions, typical issues in analog communication systems. Optical subcarrier modulation and RF power amplification are the major sources of non-linearities in RoF systems which can be caused by the non-linear characteristics of the microwave

and optical components in the system. Non-linearities can produce spurious signals which can coincide with the useful RF signals and degrade them, thus reducing the performance of the transmission system. Therefore, there is a justifiable need for the suppression of these non-linearities, i.e. linearization, to make RoF transmission systems more robust.

1.2 Optical Subcarrier Modulation

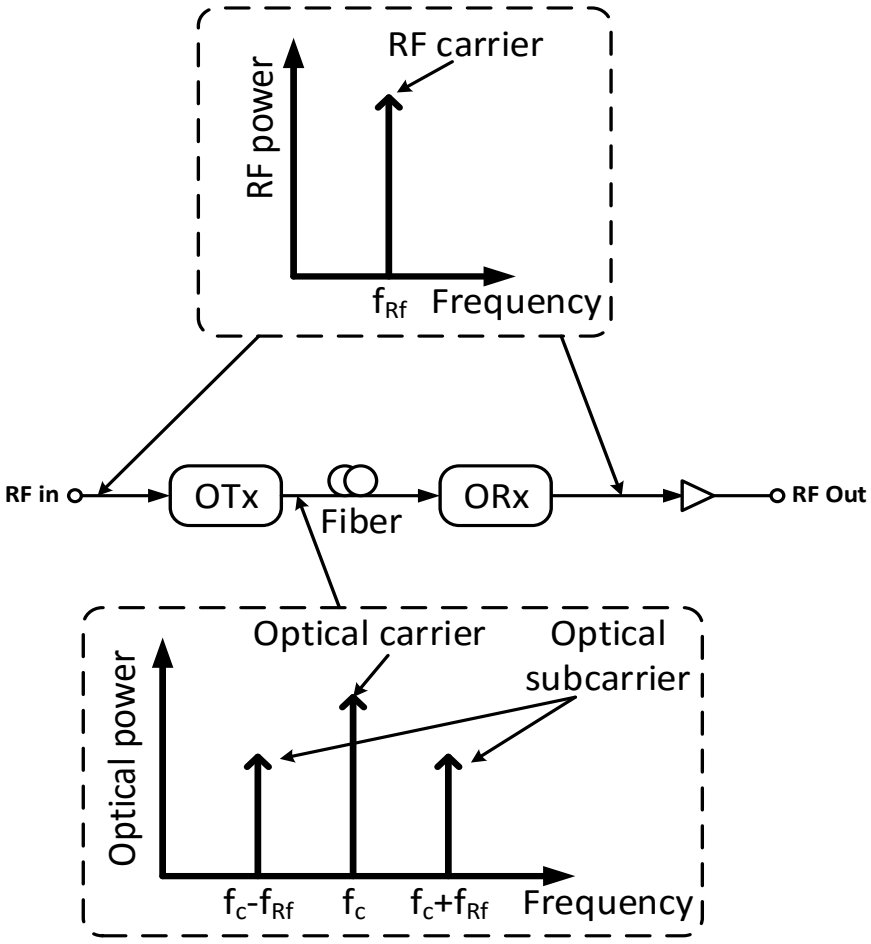

Figure 1-3: Optical subcarrier modulation principle

Figure 1-3 shows the process of optical subcarrier modulation. The optical carrier is modulated with RF signal in the OTx. This way, the RF signal in the RF domain is carried by the optical subcarriers in the optical domain to transfer from the OTx to the ORx. At the ORx, the signal is converted back to the RF domain before distribution. Optical subcarrier modulation can be carried out either by (a) direct modulation of a laser, or (b) external modulation of a CW laser

with an EAM or a MZM. Figure 1-4 shows both processes. Direct modulation can be cheap and simple but compared to external modulation, it is susceptible to higher chirp which can give rise to Chromatic Dispersion (CD) effect, a phenomenon that happens when lights at different frequencies travel in the optical spectrum at different velocities so that their arrival times at the ORx are different. Moreover, external modulation provides for higher bandwidth than direct modulation.

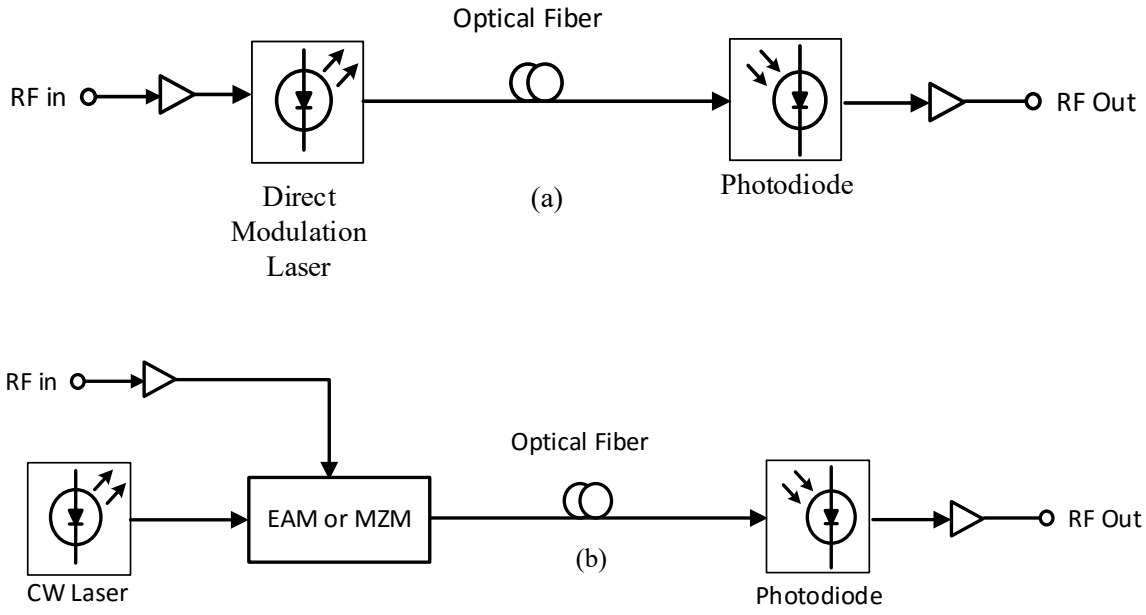

Figure 1-4 : (a) Direct modulation, (b) External modulation

As can be seen from Figure 1-3, optical subcarriers occupy more bandwidth than RF carrier because of double sideband modulation (DSB). Therefore, they are more prone to CD and non-linear distortions because larger bandwidth gives the capacity to transmit more carriers. High data rates make CD severe, resulting in errors and loss of information. To mitigate the effect of CD, single sideband modulation (SSB) [5]-[7] and also use of dispersion compensating fiber (DCF) [8]-[9] has been investigated. Figure 1-5 shows both DSB and SSB.

Optical single sideband modulation can be performed by carefully biasing the two RF inputs of a MZM and by controlling the phase difference between them. Compared to DSB, SSB generates one optical sideband which occupies half the modulation bandwidth of DSB and

therefore results in the reduction of CD. DCF is another solution to reduce CD because DCF has negative dispersion coefficient which induces dispersion to compensate for those induced by SMF.

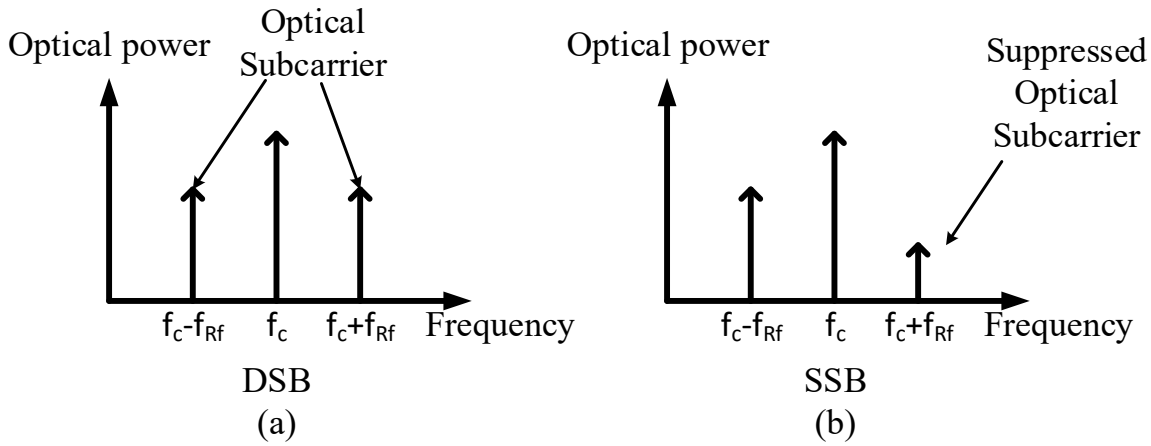

Figure 1-5: (a) Double sideband modulation (DSB), (b) Single sideband modulation (SSB)

1.3 Nonlinearities in RoF transmission systems

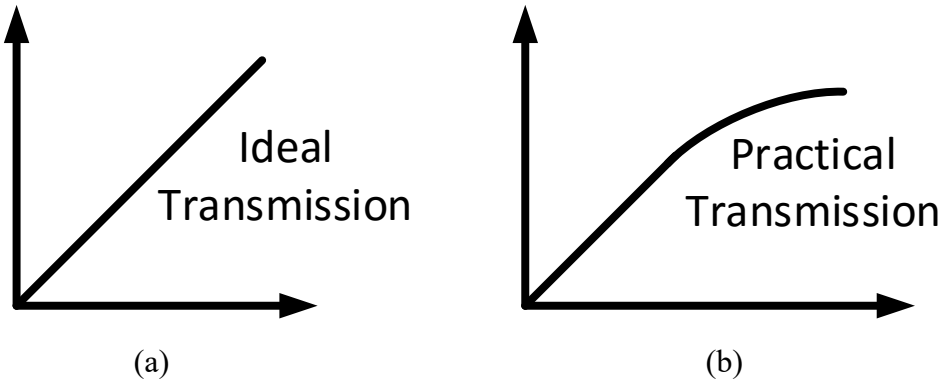

Figure 1-6: (a) Ideal transmission, (b) Non-linear transmission, in RoF transmission systems

The design principle of RoF transmission system is that transmission should be linear, i.e. the ratio of RF power output to RF power input is contant as shown in Figure 1-6 (a). However, in reality, it is impossible to achieve. At high RF input power, the tramission is always non-linear as shown in Figure 1-6 (b) and also suppressed. This non-linear behaviour at high RF input power gives rise to non-linear distortions which gets transmitted with the actual RF signals. Therefore, the nonlinearities need to be suppressed to achieve better transmission. The nonlinearities generated in RoF transmission systems are harmonics and intermodulation distortions. Harmonics

are components generated at the integer multiples of the fundamental frequencies and intermodulation distortions are components generated when two or more adjacent frequencies are transmitted in RoF link as shown in Figure 1-7. In a typical RoF transmission system, source of nonlinearities in the RF domain can be from the Power amplifier (PA). Nonlinearities in the optical domain, such as Four-Wave mixing, Cross-absorption modulation, and Cross-polarization rotation, happens because of the electro-optical modulators, semiconductor optical amplifiers (SOAs) and photodiodes (PDs).

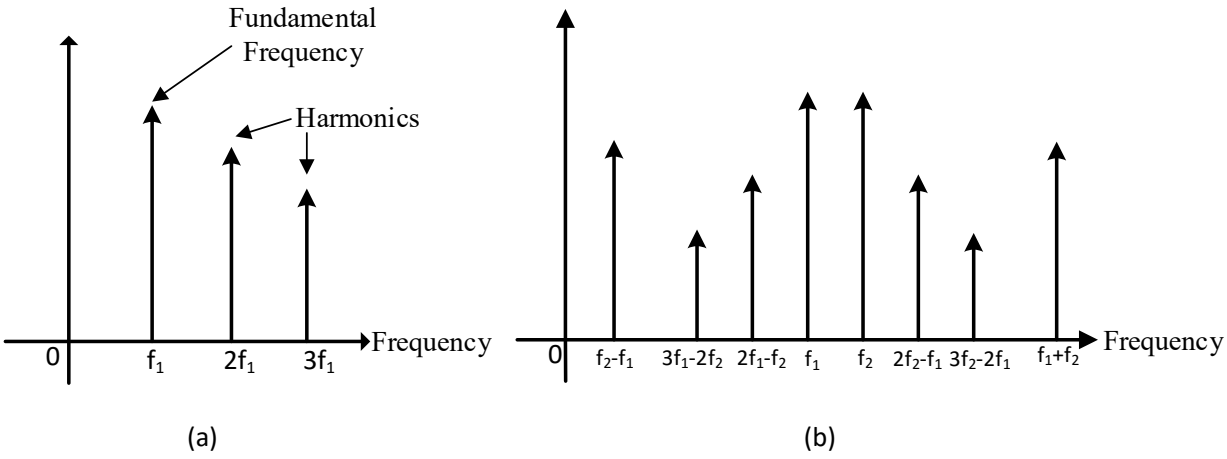

Figure 1-7: (a) Harmonic distortions, (b) Intermodulation distortions

For mathematical analysis of IMD, Taylor series can be used as shown in equation (1.1) to model the nonlinearity in RoF transmission systems [10].

$$v_0 = a_0 + a_1 v_i + a_2 v_i^2 + a_3 v_i^3 + a_4 v_i^4 + a_5 v_i^5 + \cdots \tag{1.1}$$

where input and output powers are denoted by v_i and v_0 and the coefficients are represented by a_i.

When two input signal sources at frequencies f_1 and f_2 in close proximity are applied, then,

$$v_i = V_0(\cos \omega_1 t + \cos \omega_2 t) \tag{1.2}$$

where $\omega_i = 2\pi f_i$ and V_0 is the amplitude of the input signals.

By substituting Equation (1.2) into Equation (1.1), the output of the RoF transmission system can be derived as:

$$v_0 = a_0 + a_1V_0(\cos\omega_1 t + \cos\omega_2 t) + a_2V_0^2(\cos\omega_1 t + \cos\omega_2 t)^2 + a_3V_0^3(\cos\omega_1 t + \cos\omega_2 t)^3$$

$$+ a_4V_0^4(\cos\omega_1 t + \cos\omega_2 t)^4 + a_5V_0^5(\cos\omega_1 t + \cos\omega_2 t)^5 + \cdots \quad (1.3)$$

After some trigonometric expansions and simplification of Equation (1.3), the results extracted for the third order (IMD3) and fifth order (IMD5) nonlinearities are:

3rd Order: $\left(\frac{3}{4}a_3V_0^3 + \frac{25}{8}a_5V_0^5\right)\cos(2\omega_1 - \omega_2)t$ and $\left(\frac{3}{4}a_3V_0^3 + \frac{25}{8}a_5V_0^5\right)\cos(2\omega_2 - \omega_1)t$

and

5th Order: $\frac{5}{8}a_5V_0^5\cos(3\omega_1 - 2\omega_2)t$ and $\frac{5}{8}a_5V_0^5\cos(3\omega_2 - 2\omega_1)t$

The important IMD3 components are $2\omega_1$-ω_2 and $2\omega_2$-ω_1 and the IMD5 components are $3\omega_1$-$2\omega_2$ and $3\omega_2$-$2\omega_1$ because they are the closest to the fundamental frequencies as shown in Figure 1.7(b) and cannot be filtered out. Therefore, they are the biggest contributors to nonlinearity in a RoF transmission system. The coefficients represent the amplitudes of the intermodulation products. Among all the intermodulation products, IMD2 has the largest power according to Figure 1.7(b) but falls way out of the passband of the fundamental frequencies and can be filtered out. IMD3 has the highest power among the rest of intermodulation products. Therefore, linearization technology is very important to get rid of the IMD3 and IMD5.

Among optical nonlinearities, Four-Wave mixing (FWM) is the most important in RoF transmission systems. It is a phase-sensitive process. It means the efficiency of the FWM is strongly dependent on the phase matching conditions. It is similar to the generation of IMD3. It is usually generated by EAM or SOA in the optical domain. When two lights at frequencies f_1 and f_2 are injected into an external modulator like an EAM, two more lights are generated at the frequencies of $2f_1$-f_2 and $2f_2$-f_1. The effect is shown in Figure 1-8. FWM mainly affects wavelength-division multiplexing (WDM) systems. The effects of FWM are noticeable with decreased channel spacing of wavelengths, i.e. dense WDM systems and at high signal power levels. The interference caused by FWM in WDM systems is known as Interchannel Crosstalk. The magnitude and phase

of the generated FWM lights are dependent on the intrinsic characteristics and bias voltage of the external modulator and are therefore tunable.

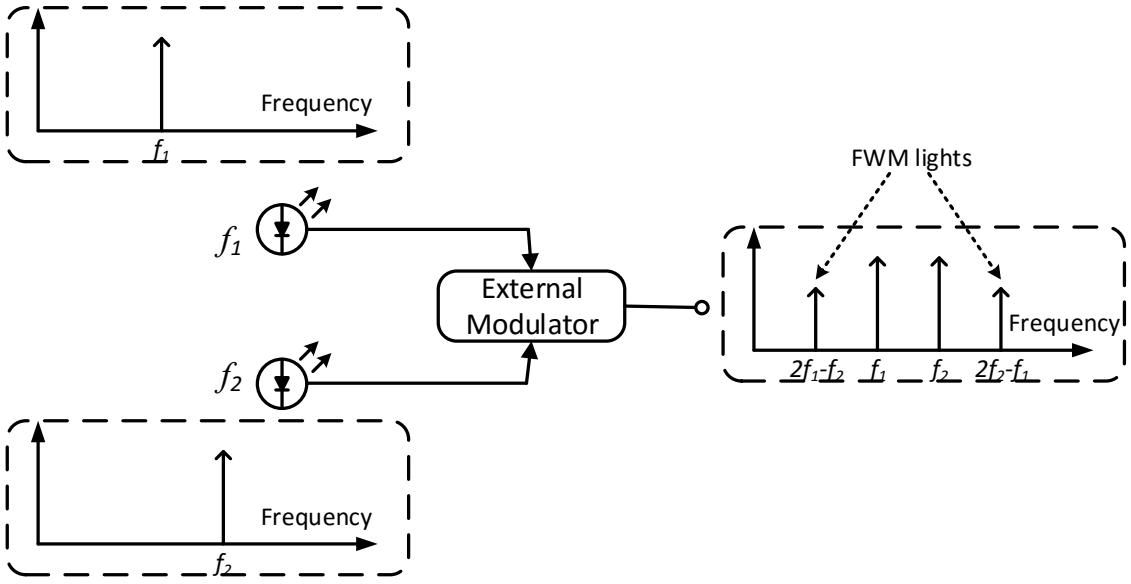

Figure 1-8: Four-Wave Mixing

1.4 Spurious Free Dynamic Range

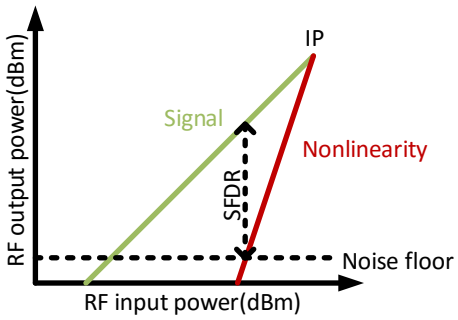

Figure 1-9: Diagram of SFDR

Spurious Free Dynamic Range (SFDR) is a measure to evaluate the linearity of a RF system. It is defined as the RF power range where the system is able to distinguish the original RF power relative to the noise level. IP is the intercept point. Figure 1-9 explains it.

1.5 Error Vector Magnitude

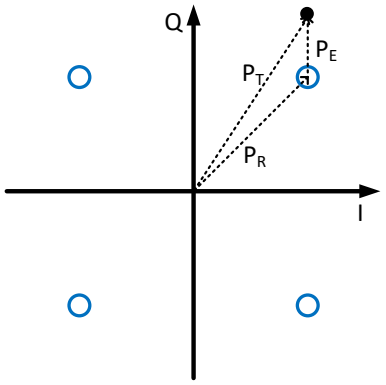

Figure 1-10: Diagram of EVM

Error Vector Magnitude (EVM) is a measure of the quality of a modulated signal. It is employed to measure the deviation of received signal from the ideal position in a constellation diagram as shown in Figure 1-10. It is measured using the following formula:

$$EVM(dB) = 10\log_{10}\left(\frac{P_E}{P_R}\right) \quad (1.4)$$

where P_E and P_R are the root mean square average power of the error vector and the reference vector, respectively.

In communication systems, Bit-error-rate (BER) is the most common performance metric used to evaluate the reliability of the system. BER assesses the full end to end performance of a system including the transmitter, receiver and the intermediate medium. If the medium between the transmitter and receiver is good and the signal to noise ratio (SNR) is high, then the bit error rate is very small and have no noticeable effect on the overall system. Bit errors mainly result in fiber optic systems from the imperfections in the components present in the link like optical driver, receiver, connectors and also by the fiber itself. Optical dispersion and attenuation can also introduce bit errors.

In [33], the relationship between BER and EVM has been investigated through simulation for different kind of modulation schemes. Figure 1-11 shows the results obtained. The simulation

results for the 16-QAM modulation scheme is of special importance to us since that is the modulation scheme used to evaluate the performance of the proposed PDC circuit for wideband signals.

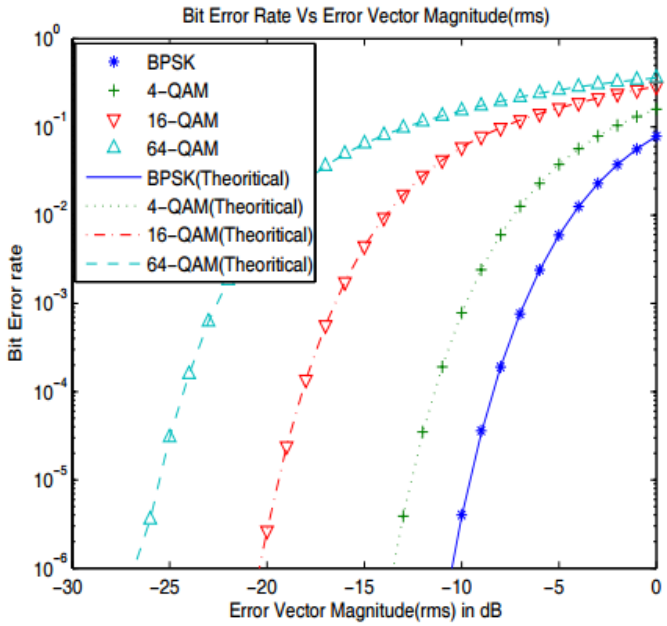

Figure 1-11: Relationships between BER and EVM[33]

From Figure 1-11, we notice that for 16-QAM modulation scheme, the BER is very small for EVM of -20 dB or less. Therefore, an EVM of -20 dB or less would be suitable for the RoF transmission system.

1.6 Literature Review of Linearization Technologies

Various linearization techniques have been proposed over the years to mitigate the effect of nonlinearities in RoF transmission systems which degrades transmission quality. Linearization means creation of opposite nonlinearities to counter the effect of those produced by the transmission system. Therefore, using linearization, it is possible to suppress the nonlinearities that gets generated in a transmission system. The main nonlinearlities to affect a transmission system are HD2, IMD2, IMD3 and IMD5. For RF signals, HD2 and IMD2 fall out of the passband and only IMD3 and IMD5 are more prominent. However, for multiband RoF transmission systems like Wi-Fi signal at 2.4 GHz or multiband orthogonal frequency-division multiplexing (MB-OFDM)

ultra wideband (UWB) signal at 3.96 GHz, IMD2 and HD2 may overlap with other signals. Optical linearization and Electrical linearization methods have been proposed as the two principal approaches as shown in Figure 1-12.

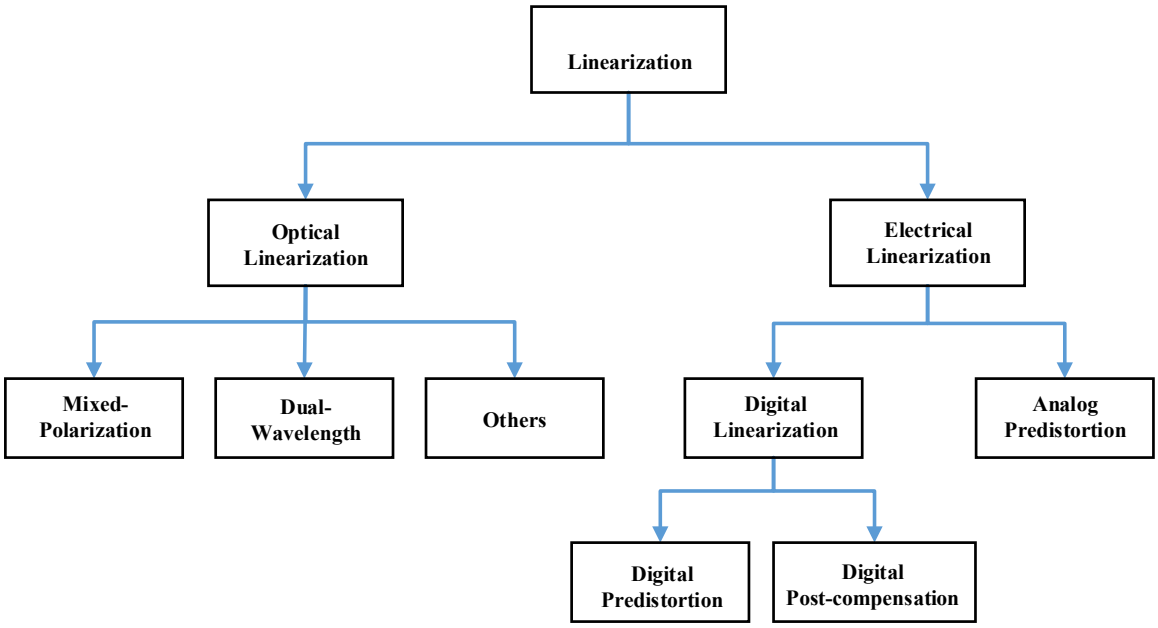

Figure 1-12: Linearization technologies [2]

1.6.1 Optical Linearization Technologies

Optical linearization depends on the principle of combining two or more nonlinear optical components and adjusting them to suppress the RoF system nonlinearities. The optical components generate nonlinearities at two separate operation points in the RoF transmission system and cancel each other when the nonlinearities are combined while keeping the RF signals mostly intact. Optical components mostly provide higher bandwidth than RF components. Therefore, they are suitable for broadband linearization of RoF transmission systems. Over the years, several optical linearization techniques have been proposed using optical components such as Mixed-Polarization (MP) linearization [11]-[15], cascaded MZMs [16]-[19], Dual wavelength (DWL) linearization [20]-[23] and others.

In the MP linearization, transverse electric (TE) and transverse magnetic (TM) transmission characteristics of a RoF transmission system are used. The nonlinear components

generated by the TE and TM transmissions are cancelled by each other if they are in antiphase. This means that the TE and TM characteristics must be different. Therefore, the RoF transmission system must be polarization dependent. Such RoF transmission system would consist of polarization dependent EAM or MZM. Both 2nd and 3rd order nonlinear distortions can be considerably suppressed by appropriately adjusting the polarization angles in this method. The RF signal may also be suppressed to some extent and the suppression would strongly depend on the TE and TM characteristics of the EAM or MZM.

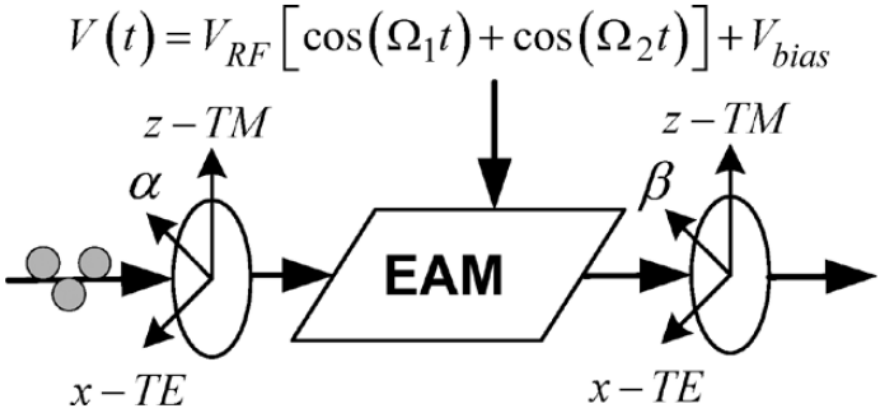

Figure 1-13: Schematic of mixed polarization [12]

In [12], Hraimel et al. proposed and experimentally demonstrated the process of optical mixed polarization linearization for an EAM modulated RoF transmission system. As shown in Figure 1-13, the polarizers before and after the EAM are set to angles, α and β respectively, with respect to the z-axis. The light signal from the first polarizer, which is set to angle α, consists of the superposition of TE and TM optical fields. The light signal will be modulated by the EAM. The EAM output will carry certain amount of intermodulation products in its TE and TM optical fields. The light then passes through the second polarizer which is set to angle β. Carefully setting the two angles in the two polarizers make them related to each other and IMD3 is suppressed while making sure the RF carriers are maximized. Experimental results showed SFDR improvement of 8.1 dB and 9.5 dB in back-to-back and after 20 km fiber transmission using this process. The stringent requirement of angle manipulation makes the linearization process highly complex.

In the optical linearization method using cascaded MZMs, the process can be done in two ways, either by cascading two MZMs is series or in parallel. Fig 1-14 shows both processes.

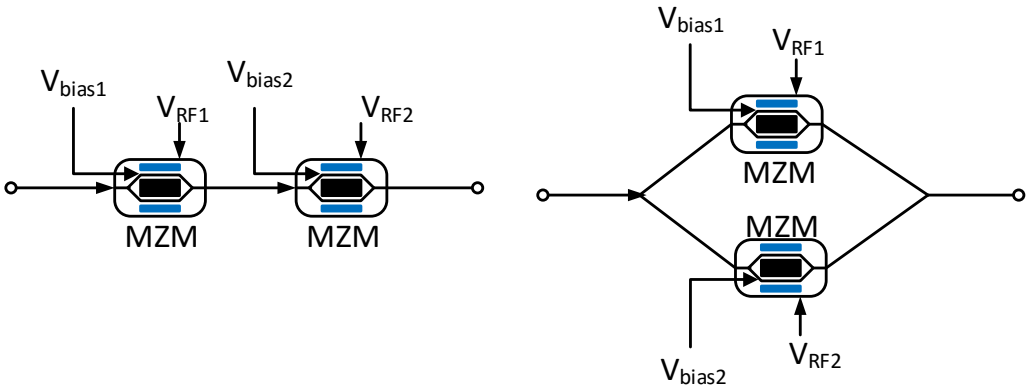

Figure 1-14: (a) Serially cascaded MZMs, and (b) Parallely cascaded MZMs

In [16], D Sabido et al. proposed a method of cascading two MZMs in series. Figure 1-14 (a) shows the process. The bias voltages of the two MZMs are adjusted along with the relative amplitude and phase of the two RF input signals at each port to achieve the suppression of the nonlinearities. The idea is for the second MZM to generate an IMD3 which can compensate for that introduced by the first MZM. Since the linearization is performed by the optical chips, the modulation bandwidth is not limited by the bandwidth of the electronic components. Experimental results showed up to 34 dB reduction in IMD3 using this process.

In [17], J. Li et al. proposed a method of suppressing IMD3 in RoF links by cascading two MZMs in parallel. Figure 1-14 (b) shows the technique. The process is designed to eliminate IMD3 completely by taking into consideration all the sidebands in the optical spectrum that cause IMD3. The method utilizes simple electrical signal phase control instead of digital linearization and other optical processors. Symmetrical single sideband modulation by the two MZMs is applied on the microwave signals. Experimental demonstrations showed IMD3 suppression of approximately 30 dB. The SFDR also improved by 12 dB. In both processes, it is difficult to vary the bias voltages and RF signals separately. Therefore, complexity is increased. Also, using two MZMs increase the cost of the RoF transmission system dramatically.

In DWL technique, the idea is to generate nonlinear distortion components at two wavelengths λ_1 and λ_2 so that they can cancel each other. Therefore, the transmission system needs

to be wavelength dependent. It means that the transmission characteristics of the RoF transmission system needs to be different for λ_1 and λ_2. The nonlinear components generated at different wavelengths will suppress each other if they are antiphase whereas the RF signals need to be in phase for improvement. Both MZM and EAM are suitable for this purpose because they have wavelength dependent transmission characteristics.

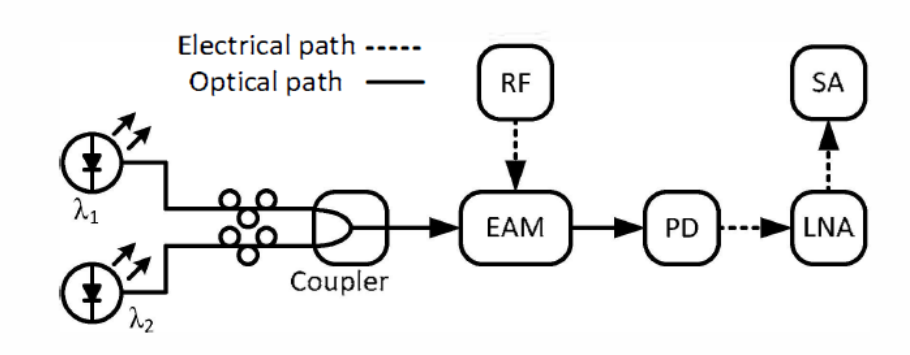

Figure 1-15: Schematic of dual wavelength linearization [23]

In [23], Zhu et al. proposed a way of linearizing an RoF link with two lasers working at different wavelengths λ_1 and λ_2. Figure 1-15 shows the setup. The wavelengths used for the two lasers in the setup were 1552.6 nm and 1510 nm, respectively. The idea is to get the nonlinearities of the two lasers to be antiphase with each other by carefully setting their power ratio. The two lights experience different modulation characteristics in the EAM and carry their own RF signals and nonlinearities because they are incoherent. Nonlinear distortions of both lasers were suppressed this way and experimental results showed that both HD2 and HD3 was suppressed by 23 dB and 2.1 dB, respectively.

Optical linearization, as a pre-distortion method, can suppress both odd and even orders nonlinearities. It covers the whole RF modulation bandwidth of the external modulator. It suffers from low loss. However, the linearization process can be complicated and expensive because of the need for multiple optical devices.

1.6.2 Digital Linearization Technologies

Digital linearization of RoF transmission links can be done in two ways: Digital pre-distortion (DPD) [24]-[25] and Digital post-compensation (DPC) [26]. The principle of this kind

of linearization is to digitally generate opposite nonlinear characteristic using a predistorter to compensate for the nonlinearity of the RoF transmission system. Memory effect in RoF transmission has to be considered when broadband signals are transmitted over the RoF system. Therefore, memoryless polynomial is not adequate to model RoF transmission systems using this process. This process uses analog to digital converter (ADC) to sample the analog signal and linearize the transmission by digital signal processing (DSP). Currently, linearization bandwidth is limited to only 20 MHz.

DPD uses the feedback of the nonlinearity information of RoF transmission system to generate a distorter. A predistorter with inverse nonlinearity characteristics is generated by sampling the input and output data of a RoF transmission system without the DPD. To approximate the predistorter, a memory polynomial is used. The input and output data of the RoF transmission system are used to train the input and output data of the predistorter. The coefficients of the memory polynomial are obtained. The coefficients of the distorter model can be extracted and the predistorter is established by using the least-square error minimization method or other algorithms.

DPC uses recursive sweep and monitors the adjacent channel power (ACP) to find the optimum coefficients of memory polynomial because the nonlinearity information of a RoF transmission system is unknown at the receiver side. Figure 1-16 shows both techniques.

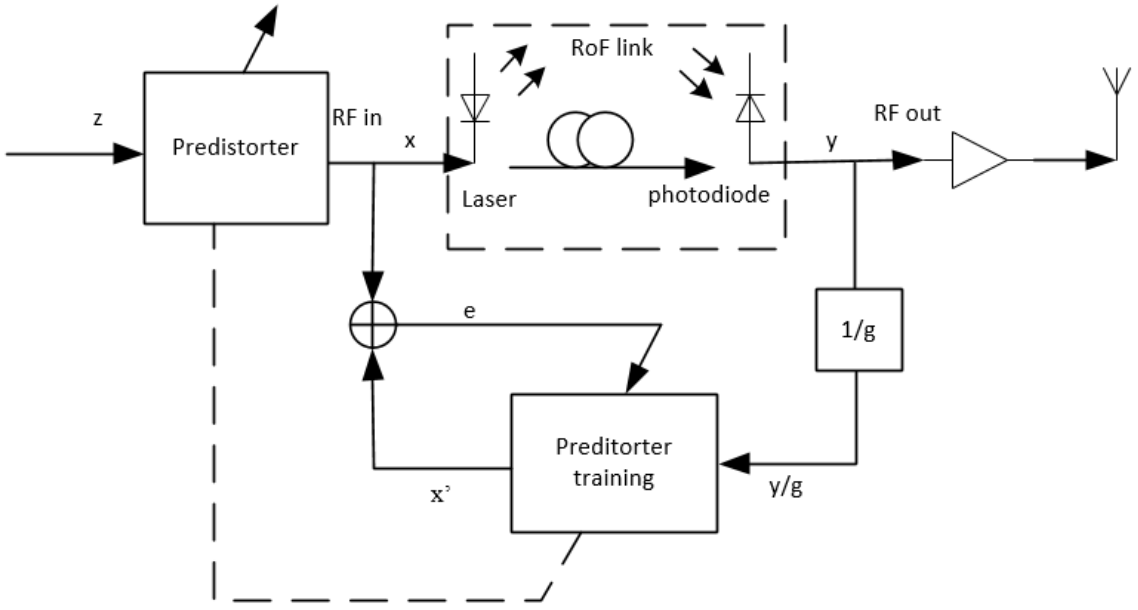

(a)

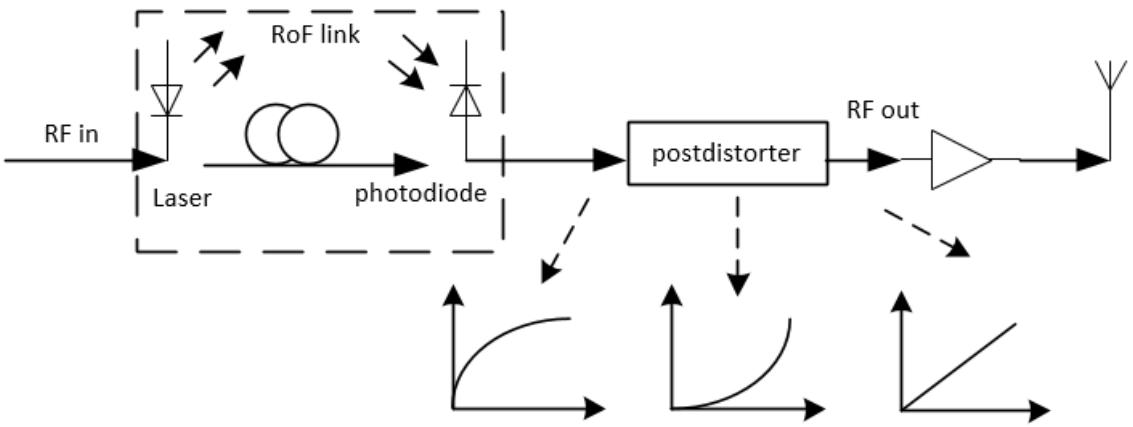

(b)

Figure 1-16 (a) Digital pre-distortion, and (b) Digital post-compensation [25]

In [25], Z. Xuan proposed a DPD method. A predistorter is trained and then verified in two experiments of directly modulated RoF transmission systems. In the first experiment, the DPD achieved more than 8 dB and 5.6 dB EVM improvement in BTB and after 10 km SMF transmission when Wi-Fi over fiber transmission system was used. In the second experiment, both Wi-Fi and ultra wideband (UWB) wireless signals were transmitted. The DPD achieved EVM improvements of 4.5 dB for BTB and 3.1 dB after 10 km SMF transmission for the Wi-Fi signal. EVM improvements of 4.6 dB for BTB and 4 dB after 10 km SMF transmission were also achieved for the UWB signal.

In [26], C. Lee et al. proposed DPC for direct laser modulation in cellular radio-over-fiber application. Through simulations, DPC was found to suppress nonlinear distortion by as much as 5 dB.

Overall, digital linearization provides the best performance as a linearization method. It is found to be adaptive. The linearization efficiency is higher and several nonlinearities can be linearized simultaneously using this method. However, it is difficult to linearize even order nonlinearities. It suffers from low bandwidth and high costs limit its practical use. Most of the broadband digital linearization is done using offline signal processing with a computer because of the issue of synchronization.

1.6.3 Analog Pre-distortion

Analog pre-distortion is the most commonly used linearization technology in RoF transmission systems. Figure 1-17 shows the principle behind analog pre-distortion.

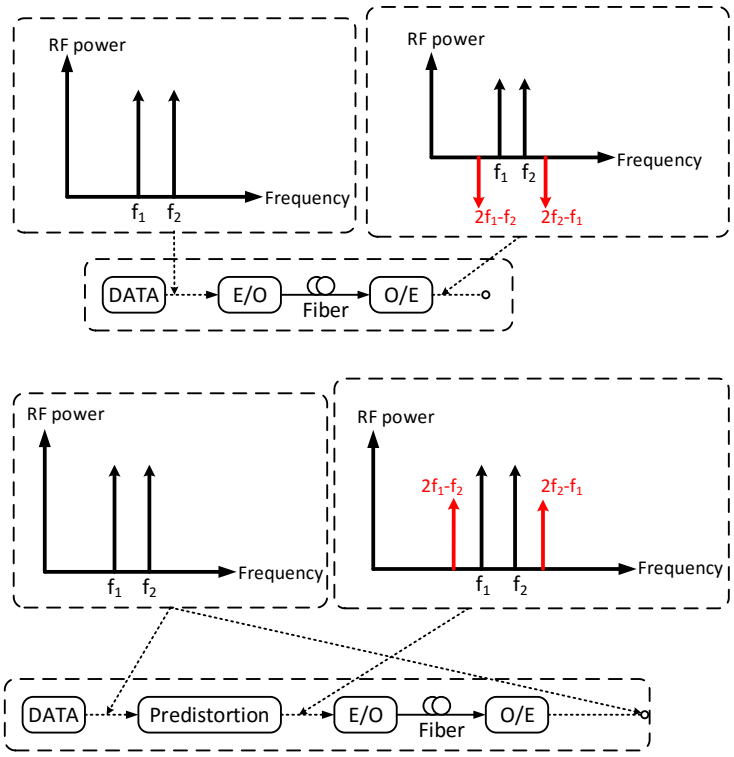

Figure 1-17: Analog pre-distortion principle [2]

As can be seen from the top part of Figure 1-17, nonlinearities are produced by optical subcarrier modulation in a RoF transmission system. The IMD3 generated is anti-phase with the original RF signal, as is usually the case because EAM or MZM in RoF transmission systems are commonly biased that way. The lower part of Figure 1-17 shows the linearization principle of a PDC. The IMD3 generated by the PDC is inphase with the RF signal due to its intrinsic characteristics. Therefore, the nonlinearities generated by the PDC and the RoF transmission system cancel each other. RF signals are mostly unaffected although some loss may occur. For broadband operations, the phase and magnitude must be precisely maintained for the PDC throughout the entire band. The acceptable phase difference between the RF signal and IMD3 should be no more than 10°. Some components in the circuit, especially capacitors and inductors, can induce phase shift. The magnitudes of the RF signal and IMD3 should be consistent for the

whole passband depending on the S_{21} of all the components, connectors, and the design of the circuit.

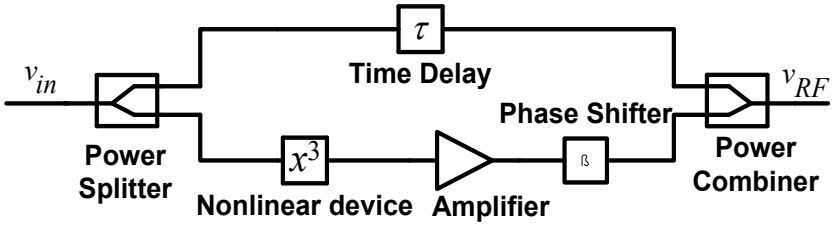

Figure 1-18: Traditional pre-distortion circuit [27]

Figure 1-18 shows a traditional pre-distortion circuit block. The input signal gets divided into two paths. One path induces a time delay while the other path contains nonlinearity generating components. At the output, the signals are combined using a power combiner. The amplifier and the phase shifter are used to adjust the magnitude and phase of the pre-distortion signal. Using this process, it is possible to achieve good cancellation of IMD3. However, the use of extra RF components like amplifiers and phase shifters can cause problems. Amplifiers are prone to generating nonlinearities of their own and phase shifters are narrowband components so they are unsuitable for broadband applications. Also, the use of two paths make it necessary to maintain a very precise time delay or the circuit can end up being a total failure. This sensitivity can be of concern for real circuit implementation of high frequency broadband systems.

In [27], Shen et al. proposed and designed a pre-distortion circuit without the use of amplifier or phase shifter as shown in Figure 1-19. It used diodes as predistorter in anti-parallel combination to generate only odd order non-linearities for pre-distortion. Quarter wave transformers were used for impedance matching.

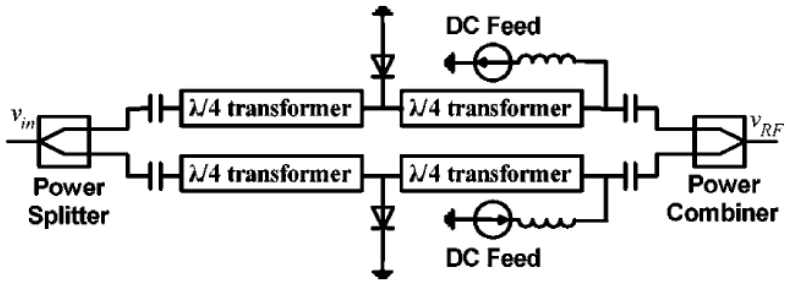

Figure 1-19: Anti-parallel diode based pre-distortion circuit [27]

The circuit was designed for linearization in MB-OFDM RoF transmission systems. Experiment results showed more than 7 dB suppression of IMD3 and 11 dB SFDR improvement over 1.7 GHz transmission bandwidth. The PDC was also evaluated in a RoF transmission of MB-OFDM UWB signals from 3.168 GHz to 4.752 GHz. Experimental results showed that EVM was improved by ~1 dB for both BTB and after 20 km SMF transmission.

In [28], Zhu et al. proposed a broadband analog pre-distortion circuit to linearize IMD3 generated in RoF transmission systems. The circuit is shown in Figure 1-20. The circuit consisted of dual schottky diodes and broadband resistors. Broadband capacitors and inductors in each arm worked as bias tees. A single direct current (DC) source was used to bias the dual schottky diodes.

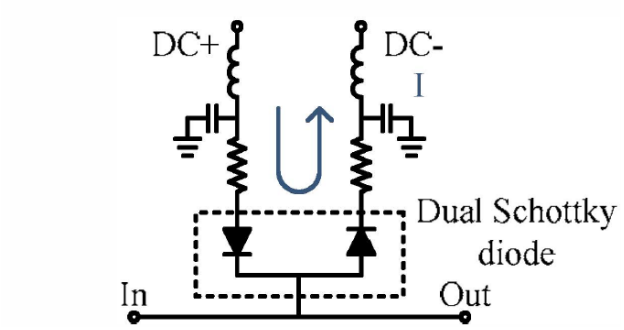

Figure 1-20: Broadband analog pre-distortion circuit [28]

Experimental results showed more than 10 dB SFDR improvement from 1 to 5 GHz. EVM was improved by 1 dB when Wi-Fi signals at both 2.4 GHz and 5 GHz were transmitted through the RoF transmission system. EAM was used as external modulator in the RoF transmission system.

Analog pre-distortion circuit offers high modulation bandwidth. It can be built simple and cheap because of the low cost of analog components. It can be made in very compact size, therefore providing ease of deployment. However, it suffers from more loss than optical or digital linearization and cannot linearize even order components. Use of nonlinear components, like amplifier, in the circuit can cause more problems because they produce nonlinearities of their own.

Over the years, there has been several attempts made to linearize both IMD3 and IMD5 simultaneously [29]-[31] in RoF transmission systems. However, there was remarkably no investigation into the use of diodes as predistorter to linearize both.

1.7 Motivation and Contribution

Cancellation of IMD3 in RoF transmission systems has been the main focus of research over the years. This is due to the fact that among odd order nonlinearities IMD3 is the most powerful and is very close to the original RF signal in the passband. Therefore, it is impossible to filter out. IMD5 is the next powerful odd order nonlinearity which also happens to be in the passband of transmission. But compared to IMD3, IMD5 is weak. However, it does have some effect on the transmission since it is also impossible to filter out because of its presence in the passband.

The main focus of this research is to develop an analog pre-distortion circuit which is capable of suppressing both IMD3 and IMD5 based on the use of diodes in anti-parallel combination as predistorter. The circuit would be designed to work in the bandwidth up to 6 GHz. It would be tested for effective suppression of IMD3 and IMD5, SFDR improvement and linearization of wideband signals in RoF transmission system.

1.8 Thesis Outline

The rest of the thesis is organized as follows:

Chapter 2 will discuss in detail about the components used in the predistortion circuit and their effect in the operation of the circuit. Some analysis on the role of diode as pre-distorter is done. The design and simulation of the proposed circuit in ADS Momentum is discussed. The s-parameter simulation results of the PDC circuit and also the simulation results for simultaneous suppression of IMD3 and IMD5 by the PDC are presented in this chapter.

Chapter 3 will discuss about the process of fabrication and experimental verification of the circuit using different kinds of signals. Experimental results wil be presented and discussions will be done on how effective the circuit is for the purpose of linearization in RoF transmission systems.

Chapter 4 will conclude the thesis and talk about future work.

Chapter 2 Proposed Analog Pre-distortion Circuit: Design and Simulation

2.1 Measurement of non-linear characteristics of EML for circuit design

An analog pre-distortion circuit has been proposed in this thesis for the simultaneous suppression of third order (IMD3) and fifth order (IMD5) intermodulation distortions in RoF transmission systems. An EML, which is an EAM integrated with a Direct Feedback (DFB) laser, is used in an experiment to measure its non-linear transmission characteristics. The EML chosen for this purpose is FLD5F20NP from Eudyna devices. The main reason for chosing an EML is that it provides extremely low wavelength chirping. Figure 2-1 shows the EML used.

Figure 2-1: FLD5F20NP (EML)

First, a steady 1.4 V DC voltage is applied to the laser section of the EML for operation of the laser. The wavelength of the laser is 1550 nm. Modulation voltage is applied through a bias tee to the modulator section (EAM) for optical subcarrier modulation. The modulated light travels through an optical fiber which is connected to an optical power meter to measure its power. The power meter used is EXPO FPM-300. By steadily changing the modulation voltage from -2.5 to 0V with an increment of 0.05V, the power of the modulated light is measured. Figure 2-2 (a) shows the experimental setup. After the measurements are done, the received power versus reversed bias voltage is plotted, which is shown in Figure 2.2 (b).

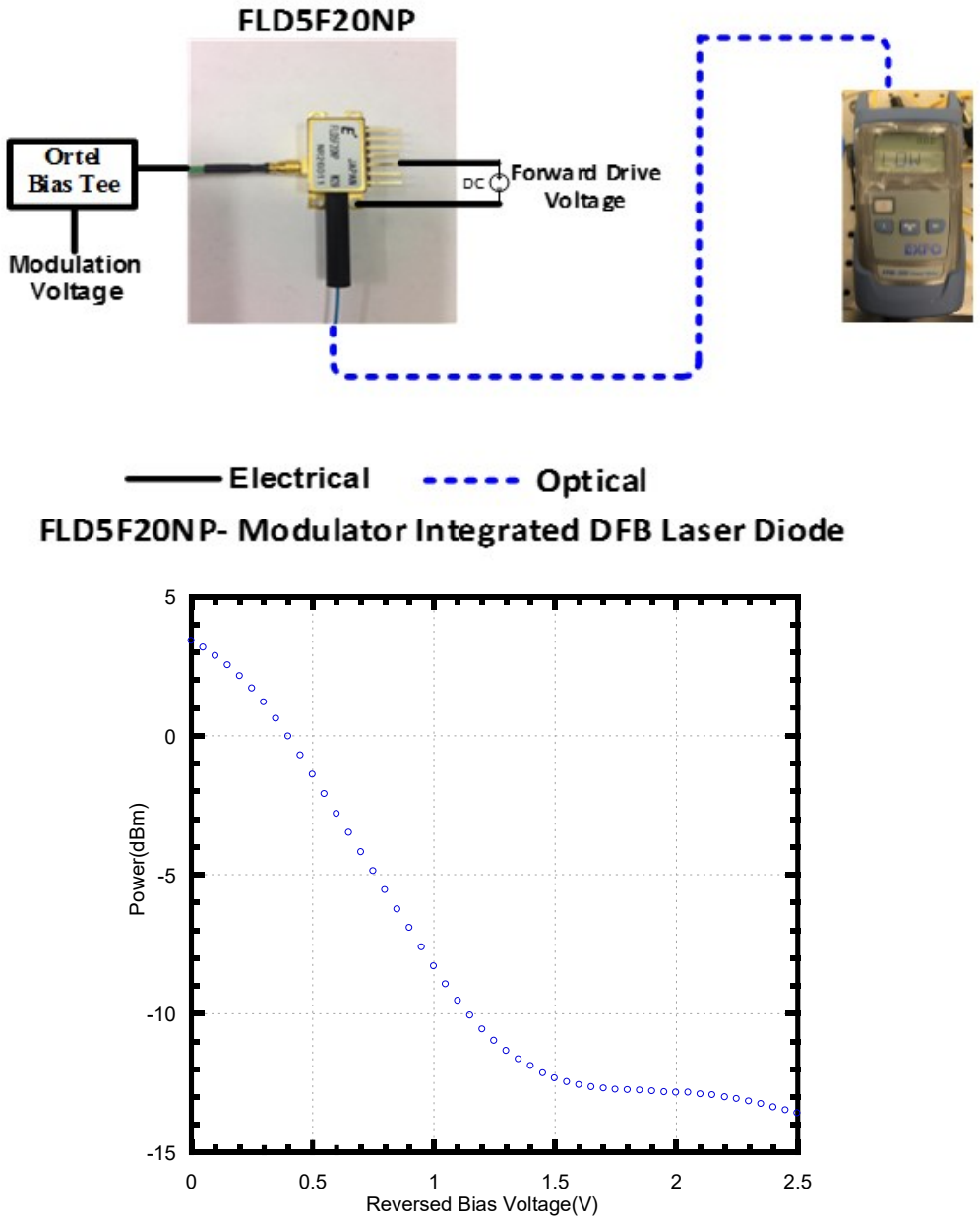

Figure 2-2: (a) Experimental setup, (b) Measured non-linear characteristics of the EML

2.2 Modelling the non-linear characteristics of EML

The measured transmission data is then entered into Matlab and the Matlab curve fitting utility is used to model the non-linear transmission characteristics of the EML into a non-linear polynomial function. Figure 2-3 shows the measured data and the 5th and 8th order polynomial

curve fitting products. The transmitted power and the curve fits are represented in dB. As can be seen from the graph, the 8th order curve fitting product fits the transmission characteristics more accurately than the 5th order product. Therefore, the 8th order non-linear polynomial model for the EML is then used to design the analog pre-distortion circuit.

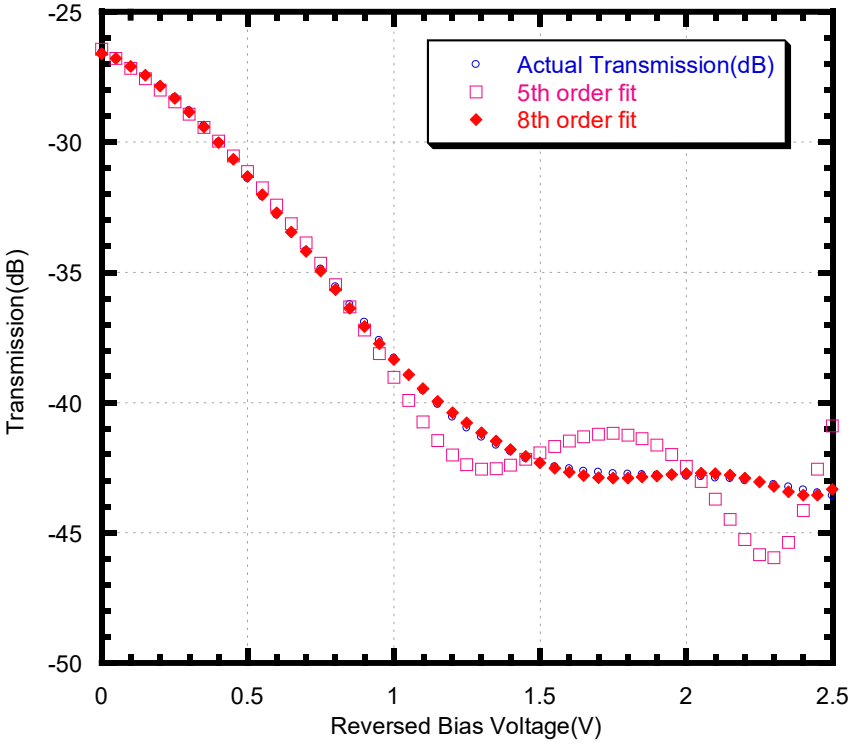

Figure 2-3: Polynomial curve fitting to model the non-linear characteristics of the EML

Equation (2.1) represents the 8th order curve fitting equation for the non-linear characteristics of the EML and the value of the coefficients are given in Table 2.1.

$$P = p_0 + p_1V + p_2V^2 + p_3V^3 + p_4V^4 + p_5V^5 + p_6V^6 + p_7V^7 + p_8V^8 \quad (2.1)$$

where V is the reversed bias voltage to the EAM.

p_0	p_1	p_2	p_3	p_4	p_5	p_6	p_7	p_8
0.0022	-0.0015	-0.0100	0.0235	-0.0234	0.0128	-0.0039	6.33×10^4	-4.085×10^{-5}

Table 2.1: Coefficients of the 8th order curve fitting polynomial

From Figure 2-3, it can be observed that modulation voltages between -1.1 V and -0.4 V are suitable in terms of the accuracy of the curve fit and also in terms of modulation efficiency. For modulation voltage below -1.1V, the insertion loss is very high and for voltage above -0.4 V the modulation efficiency is low. A modulation voltage close to -0.4V is preferable since the transmission is high around that voltage. For the experiments performed using this EML, a modulation voltage of -0.5V has been applied to the EAM, the results of which will be presented in Chapter 3.

2.3 Design and simulation of the pre-distortion circuit

The 8th order curve fitting coefficients are then used to emulate the non-linear characteristics of the EML in Advanced Design System software and a pre-distortion circuit (PDC) is designed to counter the non-linearities of the EML. ADS Momentum is extensively used as the simulation tool to design the circuit. Figure 2.4 shows the schematics of the proposed pre-distortion circuit. The circuit is similar to the one proposed in [28] except for the fact that instead of using a single chip with two diodes in anti-parallel combination, the proposed circuit has two separate diodes in two branches in anti-parallel combination. The reason for using two diodes separately is that there was no single chip anti-parallel combination package available for the diode that was chosen to build the PDC. RF signals are split into the two branches using a power divider. The power divider could be a source of phase mismatch between the two branches but extensive simulations were run to make sure the phase mismatch is kept at a minimum. Therefore, degradation of the PDC performance was avoided. Also, the proposed circuit has been optimized to suppress the IMD5 generated by the EML in addition to the IMD3 which was not investigated in [28]. The bias current through the diodes are carefully tuned to achieve suppression of both IMD3 and IMD5 simultaneously as much as possible while keeping in mind not to degrade the fundamental signal. Compared to the diode based PDC circuit in [27], the proposed PDC circuit doesn't need to use quarter-wave transmission lines for impedance matching, thereby reducing the size of the circuit dramatically. Not using quarter-wave transmission lines can cause some power loss but simulations and later experimental verification showed that the effect is minimum. Also, the proposed PDC circuit needs only one DC bias current source for both the diodes compared to two sources needed for the PDC in [27].

The input and output ports of the PDC are connected by a microstrip trasnsmission line with a characteristic impedance of 50 Ohms. The two forward biased diodes are arranged in an anti-parallel combination to form a push-pull structure so that even order non-linear components produced by the diodes are eliminated. RF broadband resistors are connected to each diode in series. The inductor and capacitor combination in each branch act as bias tees. One DC current source is used to bias both the diodes by connecting through the test points. The series resistors and the DC bias current to the diodes are tuned to maintain the power ratio and the magnitude and phase of the predistortion signals. Once the circuit is fabricated, the series resistance becomes fixed and only the DC bias current is tuned to control the predistortion signals generated by the PDC. Simulations in ADS showed that 100 Ohm resistance for each of the RF resistors is a suitable value for the operation of the PDC circuit. Therefore, the circuit uses 100 Ohm RF resistors.

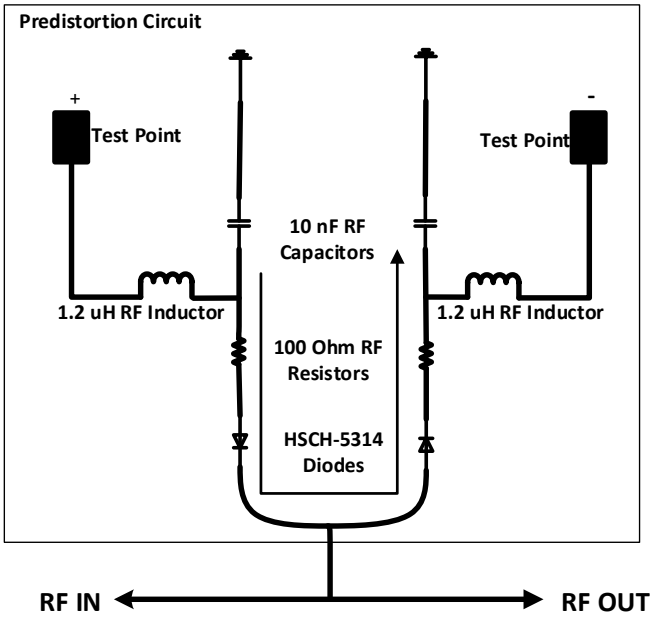

Figure 2-4: Schematic of the proposed pre-distortion circuit

The diodes used in the circuit are from Avago Technologies. The model is HSCH-5314. They are beam-lead silicone schotkky diodes. Table 2.2 shows the spice parameters for the diode [32]. A few different diode models were used in simulation to measure the performance of the PDC. While some of them showed similar level of performance during simulations, the final choice for the diode used in the circuit came down to availability and economics. Some of the diodes were not in production any more while some were available in bulk packaging only, which

made them very expensive to acquire. Most of the bulk packaging options were available in reels of hundreds or thousands of diodes. The acquisition cost for these diodes would run into thousands of dollars. Only a few diodes were needed to test the PDC while keeping the procurement costs for the equipment as low as possible. Therefore, a limited amount of diodes were acquired to build a PDC prototype. The diodes are the kernel of the pre-distortion circuit. They allow fundamental signal to flow through them. They also simultaneously generate the predistortion signals. The reason for choosing beam-lead schottky diodes is that they have smaller anode compared to regular schottky diodes. The smaller anode gives low zero bias capacitance and series inductance which is suitable for broadband applications.

$$I = I_s(e^{\beta V} - 1) \tag{2.2}$$

Equation (2.2) shows the mathematical expression for the I/V characteristics of the junction of a schottky diode where I_S is the saturation current, β is the inverse of the threshold voltage V_T and $\beta = 1/V_T = q/\eta KT$. In the expression for β, q is the electron charge, K is the Boltzmann's constant, 1.37 x 10^{-23} J/K, T is the absolute temperature in Kelvin and η is the ideality factor which accounts for the unavoidable imperfections in the junction.

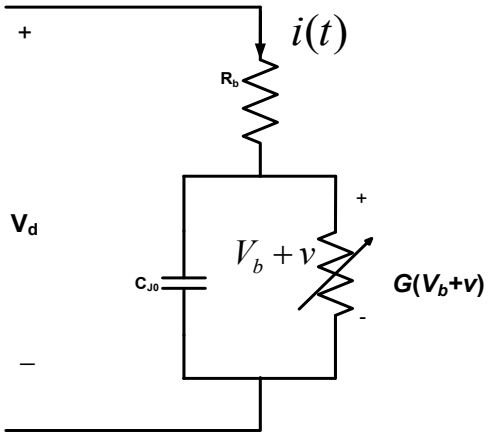

$$G(V_b + v) = \frac{i(t)}{v(t)} = g_1 + g_2 v(t) + g_3 v^2(t) + g_4 v^3(t) + g_5 v^4(t)$$

Figure 2-5: Traditional equivalent AC circuit of a Schottky Diode

Figure 2-5 shows the equivalent AC circuit of a schottky diode. Here, V_d represents the total DC voltage applied to the diode, I_d represents the DC current that goes through the diode, and V_b represents the voltage that is applied to the junction of the schottky-barrier. The series

resistor, R_b is responsible for the contact and current-spreading resistance. $C_j(V)$ and $G(V)$ are the junction capacitance and conductance. Both $C_j(V)$ and $G(V)$ are bias-dependent.

For small-signal approximation:

$$V=V_b + v(t) \text{ and } V_b = v(t)$$

where V_b represents the DC bias voltage and $v(t)$ represents the AC voltage applied to the junction of the schottky-barrier diode. The I/V characteristics of the diode can therefore be expanded using Taylor series as follows in Equation (2.3):

$$i(t) = I_s e^{\beta(V_b+v(t))} = g_1 v(t) + g_2 v(t)^2 + g_3 v(t)^3 + g_4 v(t)^4 + g_5 v(t)^5 + \ldots\ldots + g_n v(t)^n \quad (2.3)$$

where, $g_1' = I_s \beta e^{\beta V_b}$, $g_2' = \frac{I_s \beta^2 e^{\beta V_b}}{2!}$, $g_3' = \frac{I_s \beta^3 e^{\beta V_b}}{3!}$, $g_4' = \frac{I_s \beta^4 e^{\beta V_b}}{4!}$, $g_5' = \frac{I_s \beta^5 e^{\beta V_b}}{5!}$ ……...…$g_n' = \frac{I_s \beta^n e^{\beta V_b}}{n!}$

Since the diodes in the PDC are connected in anti-parallel, the coefficients for the other diode are $g_1'' = g_1'$, $g_2'' = -g_2'$, $g_3'' = g_3'$, $g_4'' = -g_4'$ and $g_5'' = g_5'$. For small signal applications, the Taylor Series is expanded upto the fifth order. The non-linear conductance can therefore be represented in Equation (2.4) as:

$$G(V_b + v) = g_1 + g_2 v(t) + g_3 v^2(t) + g_4 v^3(t) + g_5 v^4(t) \quad (2.4)$$

The graph for the I/V characteristics of the diode is shown in Figure 2-5.

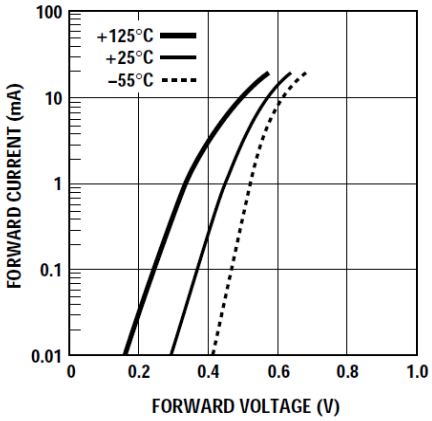

Figure 2-6: I/V characteristics of the HSCH-5314 Diode [32]

The I/V characteristics of the diode shows that as the bias current through the diode increases, so does the voltage applied to the diode. This means that changes in the bias current also changes the coefficients g_1 to g_5 in Equation (2.3).

B_v (V)	I_{Bv} (A)	I_s(A)	C_{j0}(pF)	E_G(eV)	N	R_s(Ω)	P_B (V)	P_T	M
5	10E-5	3x10E-10	0.13	0.69	1.08	9	0.65	2	0.5

Table 2.2: Spice Parameters of the diode HSCH-5314 [32]

From Table 2.2, it is seen that the zero-bias capacitance C_{j0} of the diode is 0.13 pF. The magnitude of the impedance of the zero-bias junction capacitance at 3 GHz center frequency is around 410 Ω. Compared to the series resistor R_b and the nonlinear resistance, the impedance of the capacitance at the desired frequency is large enough to be treated as an open circuit. Therefore, the capacitance can be neglected. Also, the package parasitic inductance of HSCH-5314 is 0.1 nH, which is very low. The series inductance could cause phase shift between the IMD3 and the fundamental carrier at the output of the pre-distortion circuit which would degrade the performance of the circuit. Therefore, this diode would be very suitable for the purpose.

The 100 Ohm resistors connected in series to the diode are thick film broadband chip resistors from Panasonic. The capacitors used are 10 nF ultra-broadband capacitors from American Technical Ceramics. The 1.2 μH RF inductors are broadband conical inductors from Coilcraft. Schottky diodes used in the circuit are good for operations upto 26 GHz which is much more than our target bandwidth of up to 6 GHz. Therefore, the bandwidth of the PDC circuit will be limited by the junction capacitance, parasitic capacitance, parasitic inductance and phase distortion by the diode. The series resistance of the diodes are very low at 9 Ohms. Therefore, the 100 Ohm resistors connected in series to each diode improve the S_{21} of the PDC. ADS Momentum simulations showed that 100 Ohm resistors would provide a good balance between the transmission and pre-distortion generated by the PDC. Too high resistance can make the generated pre-distortion of the PDC too weak. It would not compensate for the non-linearity of the EML in that case and performance would be bad. Without using the series resistance, the pre-distortion signal generated by the diode would be too big to compensate for the nonlinearity of RoF transmission system. The

RF capacitors work as DC block and also provide good connection to the ground for RF signals. For all the components in the circuit, manufacturer provided s-parameter files were used in simulation so that the simulated results can be as close to real world situation as possible. Figure 2-7 shows the representation of the diode equivalent circuit connected to the series resistance in the predistortion circuit.

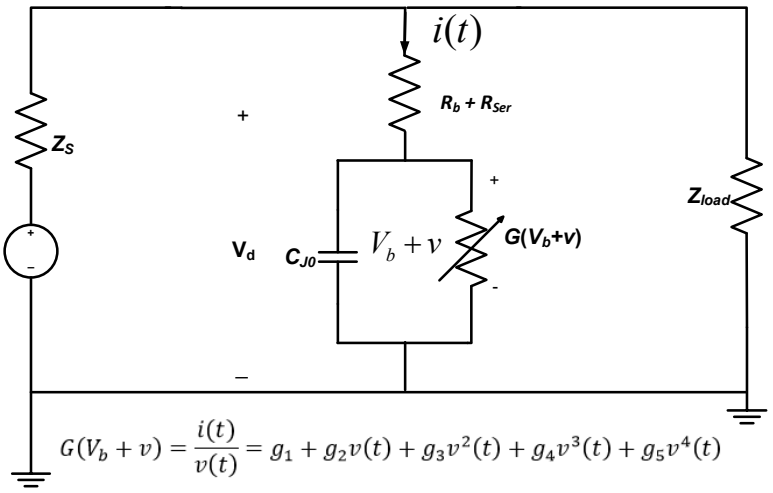

Figure 2-7: The diode equivalent circuit along with series resistance in the predistortion circuit

The PDC is simulated in ADS to determine its s-parameter characteristics. Figure 2-8 shows the simulated s-parameter characetristics of the PDC.

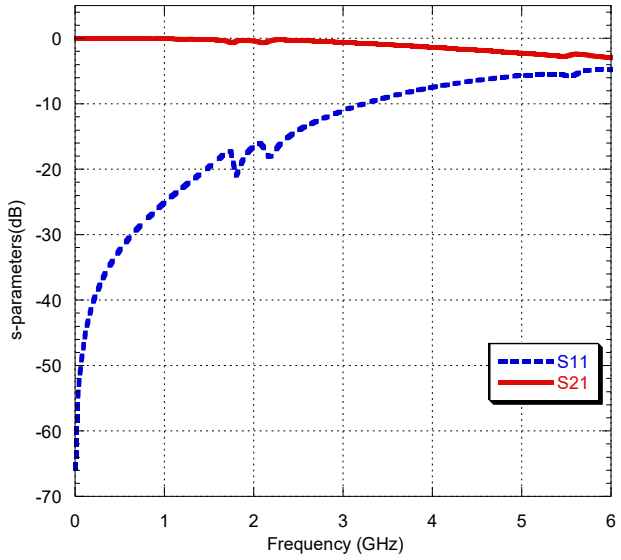

Figure 2-8: Simulated s-parameter characteristics of the proposed PDC

The proposed circuit is then simulated in ADS Momentum by applying two RF signals with frequency spacing of 2 MHz to the input port of the PDC and by connecting a nonlinear model representing the EML to the output. Extensive simulations were run to make sure the PDC work as intended to suppress both IMD3 and IMD5 generated by the EML. Figure 2-9 shows the simulated results for the simultaneous suppression of both IMD3 and IMD5.

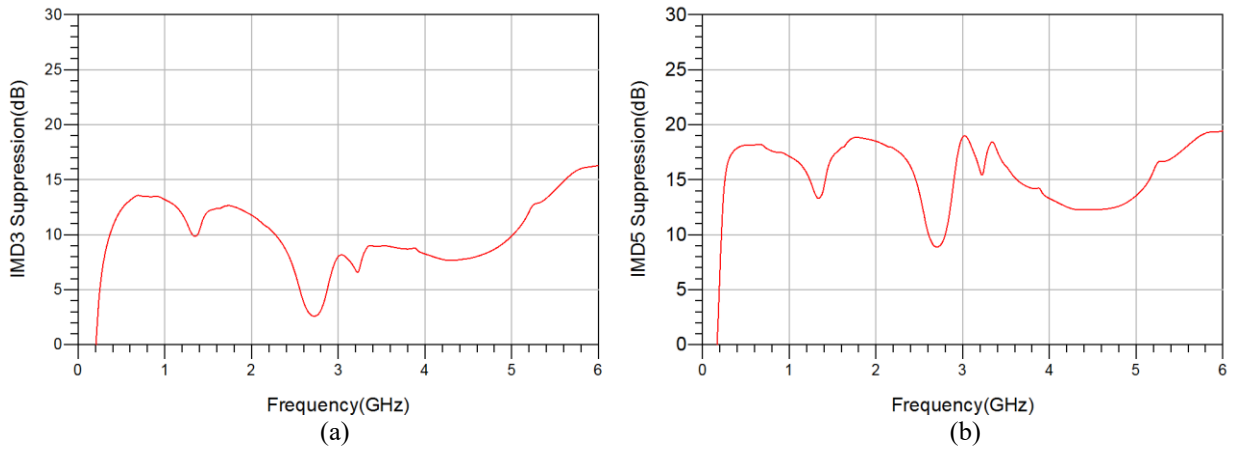

Figure 2-9: (a) Simulated IMD3 suppression, (b) Simulated IMD5 suppression

Two tones of 7 dBm each are applied to the PDC circuit which is placed right before the EML. A reversed bias voltage of 0.5 V is applied to the EML and a single suitable bias current of 2.3 mA is applied through the diodes. A lot of components like power combiner, bias tees, connectors and fibers are not required during simulations but need to be used during experiments. During experiments, all these components will introduce some effects of their own. Also, amplifiers are used during experiments which can introduce non-linearities of their own. Therefore, during experimental verification, the suppression is expected to be lower than in simualtion because certain losses will occur from the use of these components like insertion loss and fiber loss. Also, phase mismatch happens during experiments causing further loss. But these losses do not show up during simulations. Changes in temperature and pressure can also cause the transmission characteristics of the EML to fluctuate during experiments which does not happen during simulations. Therefore, change in transmission characteristics will also cause some variation in suppression during experiments. Overall, simulation results show that the PDC circuit works as intended for the purpose of simultaneous suppression of IMD3 and IMD5.

2.4 Input/Output relation of the PDC with the RoF System

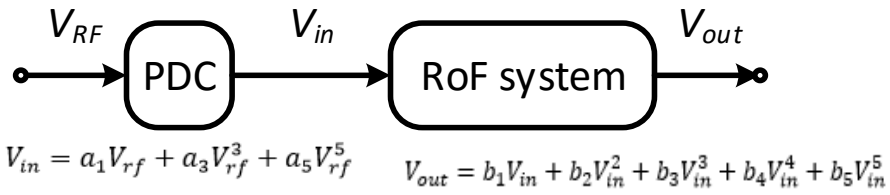

Figure 2-10: Relationship between PDC and RoF System

The principle of linearizing a RoF system with a PDC circuit is shown in Figure 2-10. The output of the PDC is the input to the RoF system. Since the PDC is symmetrical and forms a push-pull bias between its arms, therefore, all the even order components generated by the PDC are eliminated and only the 1st, 3rd, 5th and other higher odd order components remain. The ouput of the RoF transmission system after using the PDC is shown upto 5th order as follows:

$$V_{out} = a_1b_1V_{rf} + a_1^2b_2V_{rf}^2 + (a_3b_1 + a_1^3b_3)V_{rf}^3 + (a_1^4b_4 + 2a_1a_3b_2)V_{rf}^4$$

$$+ (a_5b_1 + 3a_1^2a_3b_3 + a_1^5b_5)V_{rf}^5 \quad (2.5)$$

In order to be able to completely eliminate IMD3 and IMD5, the coefficients of the V_{rf}^3 and V_{rf}^5 components in Equation (2.5) needs to go to zero.

$$a_3b_1 + a_1^3b_3 = 0 \quad (2.6)$$

According to Equation (2.6), IMD3 is completely eliminated from the RoF transmission system if the following condition is met:

$$\frac{a_1^3}{a_3} = -\frac{b_1}{b_3} \quad (2.7)$$

$$a_5b_1 + 3a_1^2a_3b_3 + a_1^5b_5 = 0 \quad (2.8)$$

By applying the condition obtained from Equation (2.7) to completely remove IMD3 into Equation (2.8) and performing some simplifications, we find that the following condition is needed to completely remove IMD5:

$$\frac{a_1^5}{a_5} = \frac{b_1^2}{3b_3^2 - b_1 b_5} \tag{2.9}$$

In Equations (2.7) and (2.9), the coefficients a_1, a_3 and a_5 are only from the diode and the coefficients b_1, b_3 and b_5 are only from the modulator in the RoF system. The coefficients b_1, b_2, b_3,.....b_n from the modulator can be extracted from the curve fitting function of the non-linear characteristics of the modulator. By refering to Equation (2.1), $b_1 = p_1$, $b_3 = p_3$ and $b_5 = p_5$. Therefore, the coefficients b_1, b_3 and b_5 are fixed in the system. In [34], Y. Shen demonstrated that the coefficients from the diode can be extracted using Volterra Series analysis and the non-linear current method, and that the coefficients are dependent on the bias current through the diode. The analysis was done upto the third order.

Simulations were performed using Matlab to find the likely range of values for a_1, a_3 and a_5 which would be suitable for the purpose of simultaneous suppression of IMD3 and IMD5. The input power was fixed for the PDC circuit and the power of IMD3 and IMD5 were found at the system output. For the IMD3 simulation, the x-axis represents the ratio of $\frac{a_3}{a_1^3}$ and for the IMD5 simulation, the x-axis represents the ratio of $\frac{a_5}{a_1^5}$. Figure 2-11 shows the simulation results.

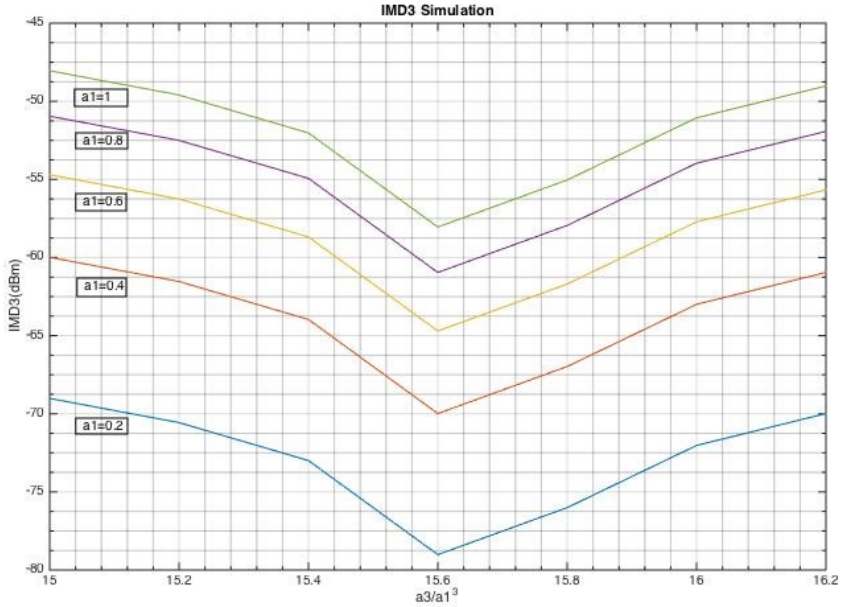

(a)

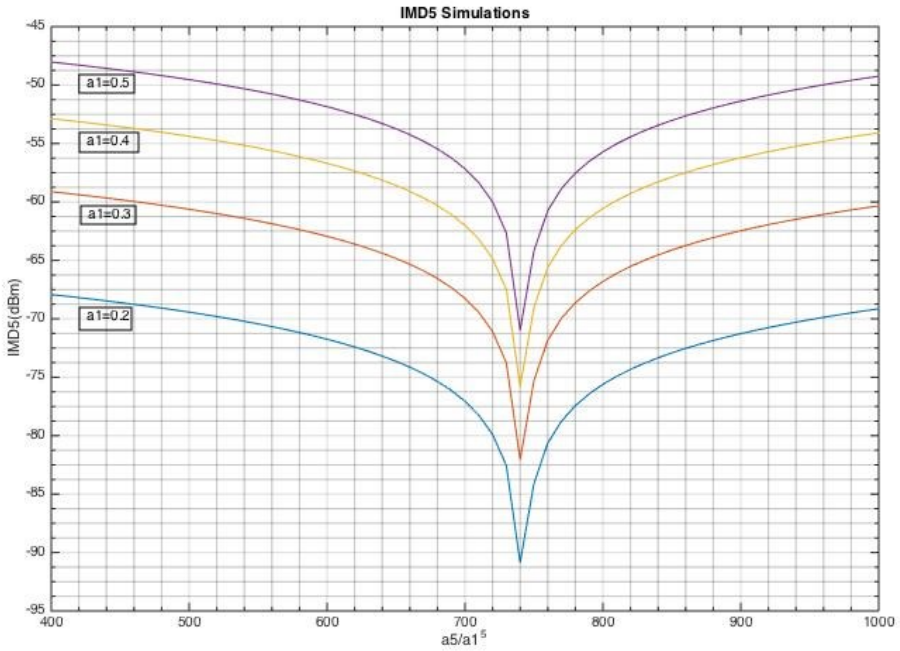

(b)

Figure 2-11: Matlab simulation results for (a) IMD3 and, (b) IMD5

In Figures 2-11 (a) and (b), the values of b_1, b_3 and b_5 were fixed by obtaining the coefficients from the 8th order curve fitting function in Equation (2.1). The simulations were run by varying the value of the coefficient a_1. A likely range of values for the power of IMD3 and IMD5 at the system output were set and the corresponding range of a_3 and a_5 respectively were obtained. The reason for choosing range of IMD3 and IMD5 values is to account for the anomalies like insertion loss or connection loss that can happen during experimental work which cannot all be predicted during simulation. The anomalies can cause the power level to be different from an ideal system. For the purpose of simulation, the range of values set for IMD3 at system output was between -50 to -70 dBm and the range of values for IMD5 at system output was between -70 to -90 dBm. From the graphs, we can observe that the effects of IMD3 and IMD5 at system output are lower for low values of a_1. As a_1 increases, so does the effect of IMD3 and IMD5. The dip in both figures happen at the ratio corresponding to the values of b_1, b_3 and b_5 obtained from the curve fitting coefficients in Equation (2.1). However, temperature and pressure changes can also cause variation in the transmission characteristics of the modulator. That can cause the values of b_1, b_3

and b_5 to fluctuate. Therefore, for practical reasons, a range for the ratios is also taken. The range for the ratio of $\frac{a_3}{a_1^3}$ in IMD3 simulation is taken between 15 and 16 and the range for the ratio of $\frac{a_5}{a_1^5}$ in IMD5 simulation is taken between 700 and 760. From the figures, we can deduce that the range of values for a_1 which works for both IMD3 and IMD5 within the specified ranges are between {0.2 to 0.5}. Based on the specified range for the ratios in both cases, the ranges for a_3 and a_5 are obtained as:

$$a_3=\{0.2 \text{ to } 2\}$$

$$a_5=\{0.22 \text{ to } 23.75\}$$

For real world applications, it is not possible to physically adjust these coefficients in diodes. Therefore, extensive simulations are performed using various diode models to find out if the characteristics of the diode exhibit the required performance in the PDC circuit. In ADS simulations, many diode models were used to analyse the performance of the PDC and suitable ones were chosen which demonstrated the ability to suppress both IMD3 and IMD5 to a reasonable extent. Then, based on availability and acquisition cost, a specific diode model was used for the fabrication of the PDC. Also, during experimental verification, the performance of the PDC circuit ensured whether the coefficients were within the specified range or not as will be demonstrated in Chapter 3.

Chapter 3 Linearization of RoF Transmission System using Proposed PDC: Fabrication and Experimental Verification

3.1 Fabrication and Performance of the PDC circuit

After successfully simulating the PDC circuit, it was sent for fabrication to the Poly-Grames Research Center at Ecole Polytechnique Montreal. The subtrate used for the prototype is Rogers RO4350B. It has a dielectric constant of 3.48 and thickness of 16.6 mil and 0.5 oz copper cladding. Two SMC connectors are soldered to the microstrip transmission line to use as input and output of the PDC. Also, two test points are added to the two arms to apply DC bias current to the diodes. The prototype of the PDC circuit is shown in Figure 3-1.

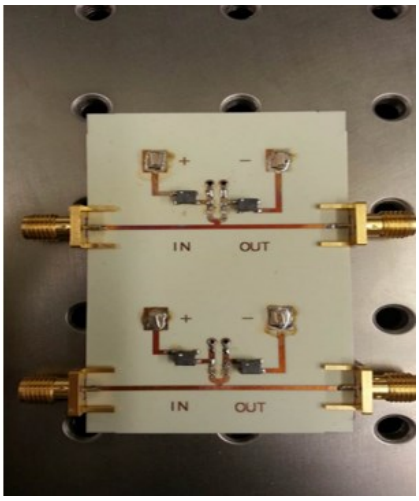

Figure 3-1: Prototype of the proposed PDC

The fabricated circuit was tested in lab to measure its s-parameter characteristics. The s-parameter results were measured using a network analyzer. Figure 3-2 shows the results obtained from lab measurements for the s-parameter characteristics and compares them to the simulated results. As can be seen from Figure 3-2, the S_{21} for the fabricated circuit is close to 0 dB for upto 3 GHz and dips to about -3 dB until 6 GHz. The experimental results almost exactly match the simulation results for S_{21}. The S_{11} is less than or equal to -10 dB upto 3.1 GHz after which it goes upto about -4 dB until 6 GHz. For frequencies higher than 3 GHz, the experimental results actually show that the fabricated circuit performs better than simulation in terms of S_{11}. Overall the S_{21} and

S_{11} performances are acceptable and the experimental results resemble the simulation results closely.

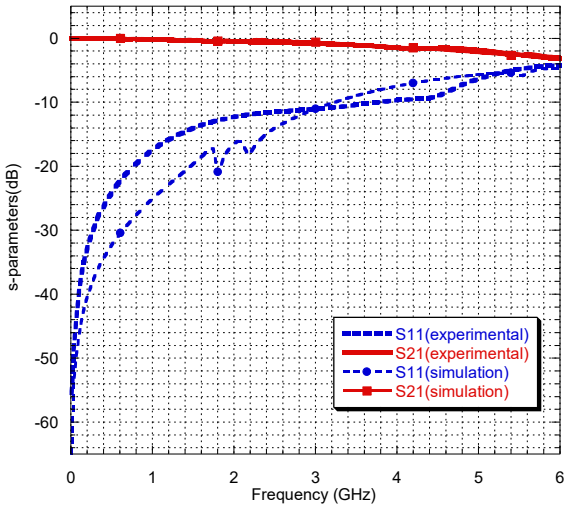

Figure 3-2: Comparison of s-parameter characteristics of fabricated circuit with simulation results

The PDC has been fabricated in big size for the ease of handling in laboratory testing. Two identical circuits were fabricated on the same board to get the luxury of having a spare circuit in case one gets damaged in any accidental mishap during tests. Also, big size test points were added to the two arms of the circuit to deliver a single DC bias current for the diodes.

For mass deployment purposes, it is possible to dramatically reduce the size of the fabricated circuit. First of all, the transmission line connecting the input and output ports can be reduced greatly in size. There would be no need to use test points to deliver DC bias current to the diodes. Therefore, the big extensions to install the test points can be eliminated. Also, the size of the SMC connectors can be greatly reduced by using smaller ones. Therefore, major miniaturization of the circuit is possible. Moreover, the circuit has been constructed with widely available parts which ensures that the cost can be minimized.

The fabricated PDC circuit is tested through a set of experiments to measure the linearization of RoF transmission system. Firstly, the PDC is evaluated with RF signals by performing a two-tone test and by measurig the SFDR improvements related to both IMD3 and IMD5. Also, to verify the linearization of wideband signals, the EVM of wifi signals transmitted in RoF system is measured first without using the PDC and then measured again by using the PDC. The EVM improvement from the two measurements are recorded.

3.2 PDC linearization for RoF transmission system using EML

The PDC is evaluated in a RoF transmission system by first using the EML, FLD5F20NP. In the first experiment, a two-tone test is performed. The schematic diagram of the experimental setup is shown in Figure 3-4.

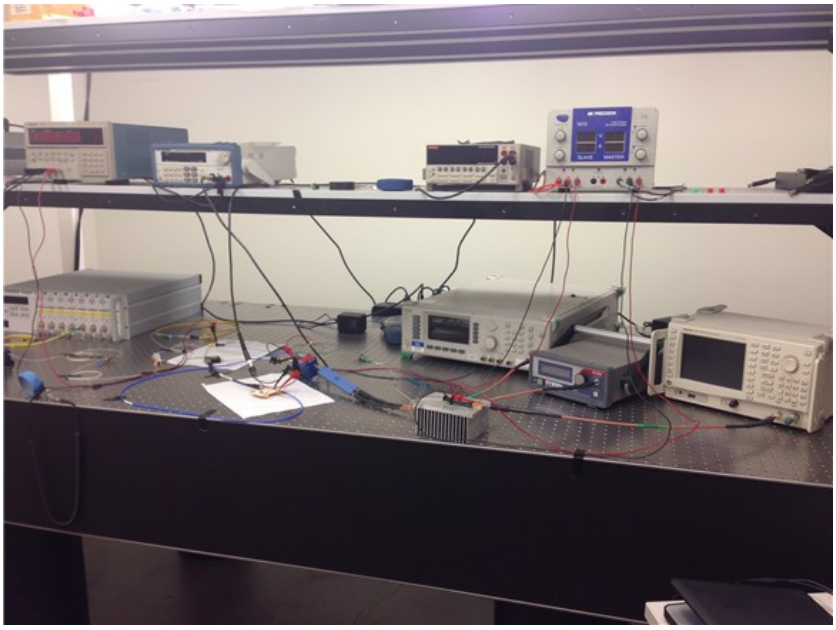

Figure 3-3: Photo of the experimental setup of two-tone test using EML

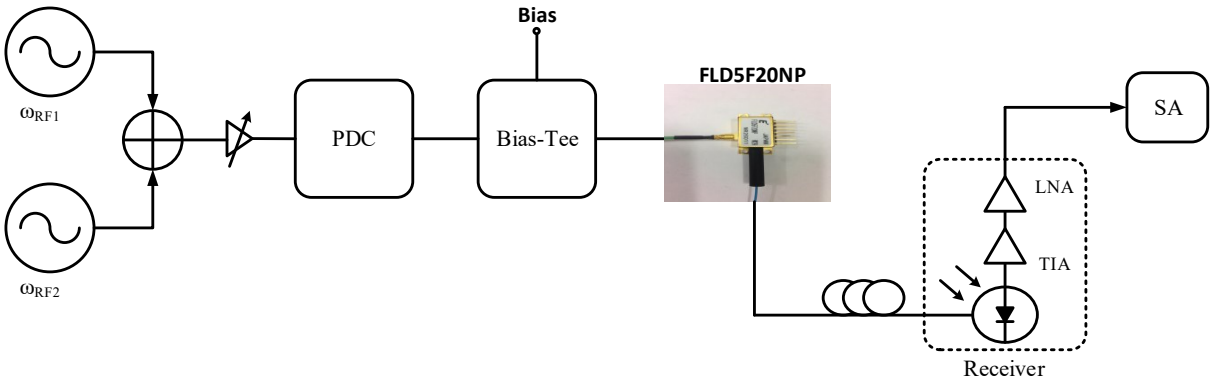

Figure 3-4: Schematic of the experimental setup of two-tone test using EML

Two signal generators generate RF signals which are combined using a broadband power combiner to give a two-tone signal with frequency spacing of 2 MHz. The signal goes through a PA ZVA-213-S+ and a variable broadband attenuator (ATT) which together forms a variable PA. The PA works in its linear region for this measurement. It has a gain of 26 dB and a noise figure (NF) of 3 dB. The PDC is connected between the variable PA and a broadband bias tee. The bias tee combines the RF signal and the reversed bias voltage for the modulator and delivers to the EML. The reversed bias voltage for the modulator is set at 0.5V which was determined through measurements to produce the best results. The DFB laser inside the EML produces a CW light at 1550 nm. The modulated light from the EML goes throught the optical fiber which is connected to an optical receiver. The receiver is a PD integrated with a transimpedance amplifier (TIA) followed by a low noise amplifier (LNA). The model number for the receiver is SCMR-100M6G-10-20-10 from Miteq. The receiver converts the received optical signal back to RF signal. The receiver is connected to a spectrum analyzer (SA) U3772 from ADVANTEST. The received RF power is measured in the SA. The resolution bandwidth (RBW) of the SA is set at 30 kHz and the video bandwidth (VBW) is set at 10 kHz. The RBW causes the RF noise floor to appear at -100 dBm during measurements. Both the RBW and VBW affect the sweep time. The noise floor for the SFDR graph is measured by setting the RBW and VBW to the lowest possible resolution.

RF signals between the power levels of -29 dBm and -6 dBm at different frequencies are generated using the RF signal generators and sent through the variable PA. The combined RF signals generated at different power levels are always at frequency spacing of 2 MHz. First the received RF powers are measured without the PDC and then they are measured with the PDC. The power levels of the received original RF signals, the IMD3s and IMD5s are measured in both cases. When the measurements are done with the PDC connected to the setup, a DC current source is used to sweep the bias current through the diodes and the power levels are recorded when a bias current reduces IMD3 and IMD5 components the most while minimizing the reduction in power levels of the original signals. The experiment is conducted for the entire target bandwidth of up to 6 GHz.

The best suppression for the IMD3 and IMD5 using the EML was achieved at 1GHz with the generated RF signals at the power level of -19 dBm and a bias current for the PDC circuit at 3.5 mA. The IMD3 was found to be suppressed by ~ 6 dB and the IMD5 by ~7 dB. The SFDRs

were also measured at frequencies from 1- 6 GHz and the SFDR improvement when using the PDC circuit to linearize the RoF transmission system was calculated. Figure 3-5 shows the SFDRs with and without PDC at 1 GHz.

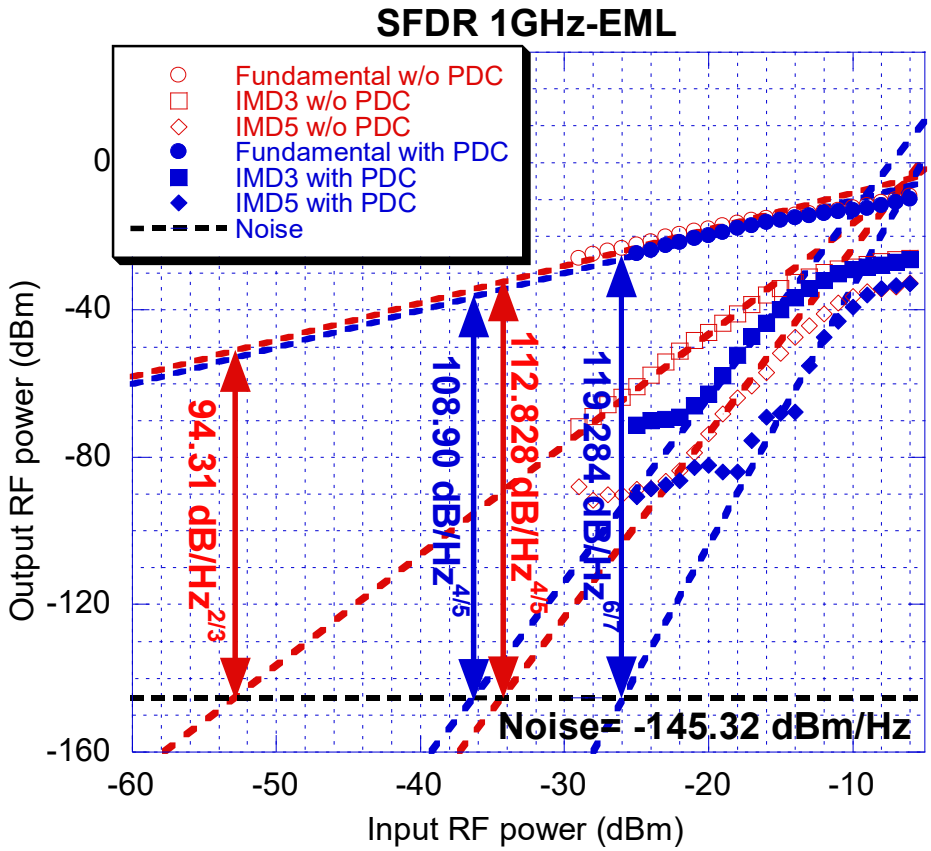

Figure 3-5: SFDR with and without PDC at 1GHz

As can be seen from the graph, at 1GHz, the SFDR related to IMD3 without using PDC is 94.31 dB/Hz$^{2/3}$ and when the PDC circuit is added, the SFDR is 108.90 dB/Hz$^{4/5}$. That is more than 14 dB improvement in SFDR related to IMD3. The IMD3 is seen as 5th order limited when PDC is used. Similarly at 1 GHz, without the PDC, the SFDR related to IMD5 is 112.828 dB/Hz$^{4/5}$ and when the PDC is used, it is 119.284 dB/Hz$^{6/7}$. That is an SFDR improvement of over 6 dB related to IMD5. Also, the IMD5 is 7th order limited when PDC is used. Lots of external factors can cause descrepancies in values obtained during measurements. Therefore, reasonably best fitting lines has been used to calculate the SFDR values. As can be observed from the graph, at low RF input power, the non-linearities produced by the system with and without the PDC flats

out. This is because at low RF input power, the non-linearity from the modulator is not continuous. But since the power level of the non-linearities are very low at those input power levels, their effect on the transmission system is not significant. Suppression of non-linearities at high RF input powers when the non-linearities themselves are strong confirms the effectiveness of the PDC circuit for the stated purpose. Also, the behaviour of the non-linearities at high input powers ensures that the IMD3 is 5th order limited and the IMD5 is 7th order limited.

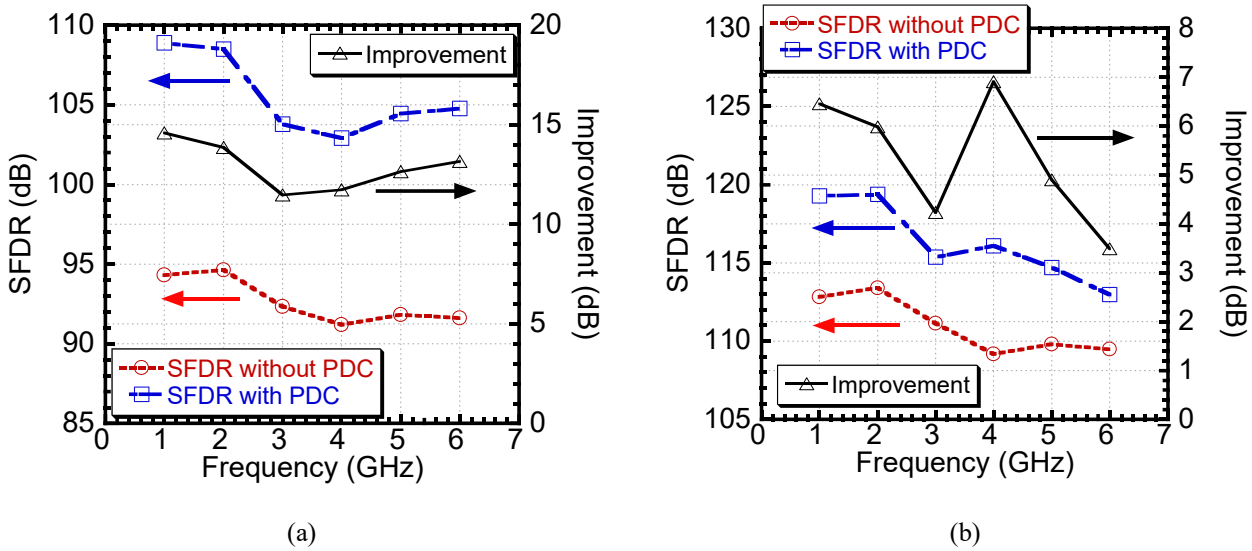

Figure 3-6: SFDR improvements related to (a) IMD3, and (b) IMD5

Figure 3-6 (a) and (b) shows the SFDR improvements related to IMD3 and IMD5 for the entire bandwidth upto 6 GHz when using the EML for modulating RF signals. As can be seen from the graphs, related to IMD3, SFDR improvement is regularly over 10 dB throughout the entire target bandwidth reaching a peak of over 14 dB at 1 GHz and the lowest of over 11 dB at 3 GHz. Related to IMD5, the SFDR improvement is over 4 dB for upto 5 GHz and dips to 3.4 dB at 6 GHz. The peak is reached at 4GHz with a SFDR imrovement of 6.9 dB and the lowest at 6 GHz with 3.4 dB. The dip in SFDR improvement related to IMD5 at 6 GHz can be because of insertion loss and noise at higher frequency. Overall, the results show that the PDC is capable of linearizing the RoF transmission system.

The RoF system is tested for linearization using PDC for wideband signals. Wifi signals at 2.4 GHz and 5 GHz are transmitted through the RoF system and the EVM is measured, first without using PDC and then again by using PDC. The EVM improvement is calculated from the

two measurements. The measurements are done for back-to-back (BTB) transmission and for transmission after travelling through 10 km single mode fiber (SMF). The long distance transmission was done to make sure if the system can work over such distances and produce noticable improvements, as is usually required in real world situations. Figure 3-7 shows the photo of the experimental setup and Figure 3-8 shows the schematic of the setup.

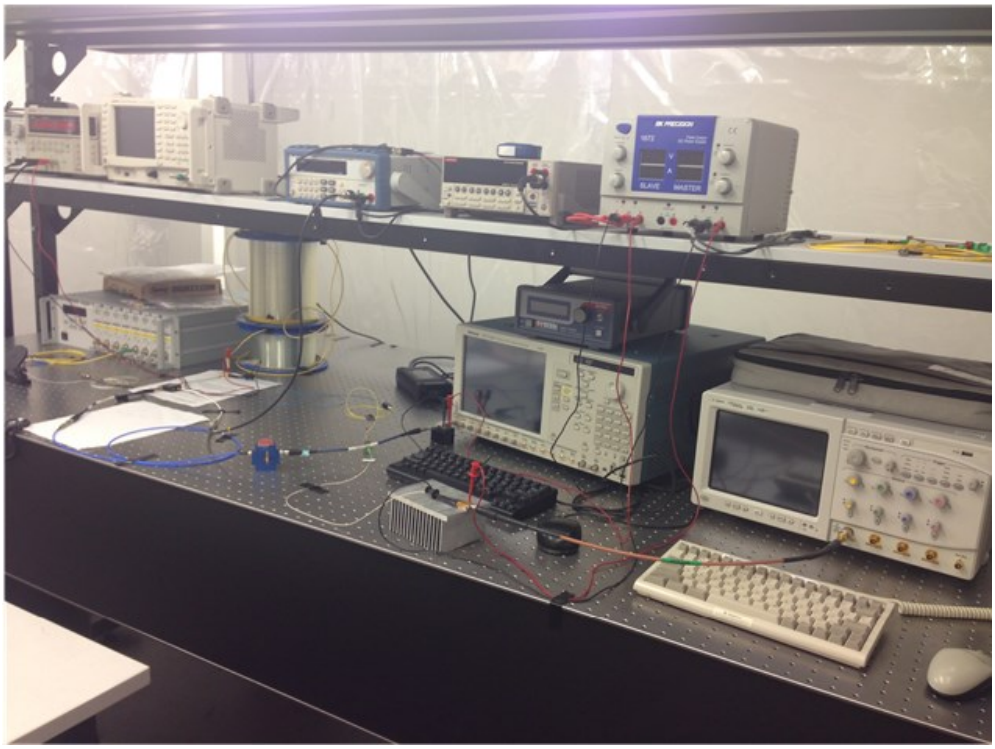

Figure 3-7: Photo of the experimental setup for Wifi signals using EML

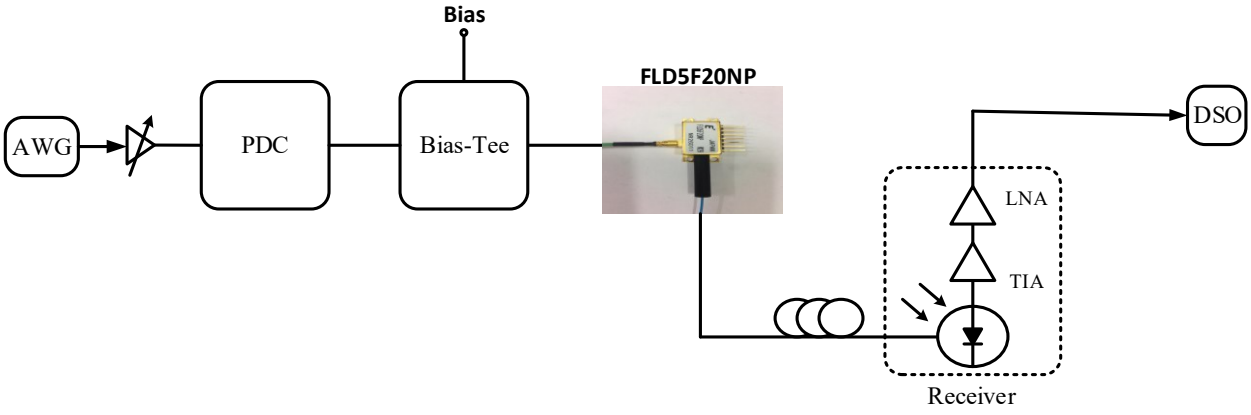

Figure 3-8: Schematic of the experimental setup for Wifi signals using EML

As can be seen from the schematic of the setup, an Arbitrary Waveform Generator (AWG) 7122B from Tektronix is used to generate Wifi signals at 2.4 GHz and 5 GHz. The signals are compliant with the 802.11a standard. The generated OFDM signals have 64 subcarriers with 16 Quadrature Amplitude Modulation (QAM). The occupied bandwidth is 20 MHz and signal rate is 36 Mb/s. The generated Wifi signals go through a PA ZVA-213-S+ and a variable broadband attenuator which together forms a variable PA. The PDC is connected between the variable PA and a broadband bias tee. The bias tee combines the generated OFDM signal and the bias voltage for the modulator of the EML and delivers to the EML. The gain of the variable amplifier before the PDC is adjusted by 1 dB step to change the RF input power to the EML. The RF input power to the EML is varied from -28 dBm to -19 dBm for 2.4 GHz and from –32 dBm to -23 dBm for 5 GHz. The modulated signal travels through the optical fiber of the EML which is connected to a PD integrated with a TIA and a LNA. A digital storage oscilloscope (DSO) 81204B from Keysight is used to receive and demodulate the Wi-Fi signals after transmission through the RoF system. For long distance transmission of the OFDM signal, a 10 km long SMF is added between the EML and the receiver. The EVMs are measured first without using the PDC and then again by using the PDC. The reversed bias voltage for the modulator of the EML is set at 0.5 V. A DC current source is used to sweep the bias current through the diodes in the PDC and is recorded when the best EVM is achieved. Figure 3-9 shows the measured EVMs at 2.4 GHz for (a) BTB transmission and, (b) 10 km SMF transmission, with and without using the PDC.

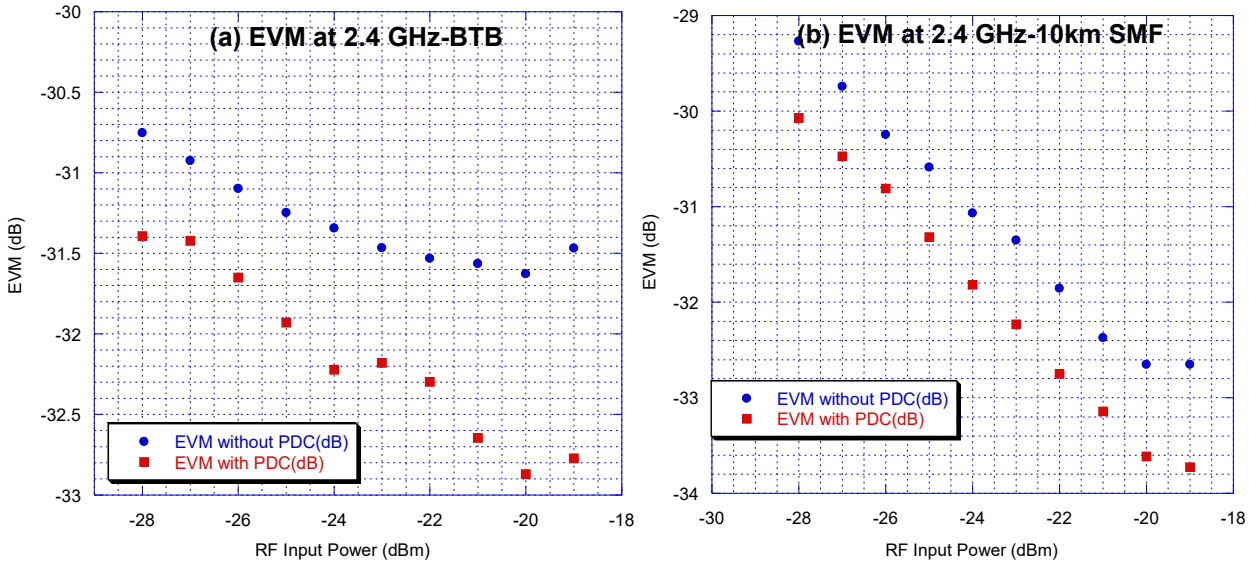

Figure 3-9: EVM at 2.4 GHz (a) BTB transmission, (b) 10 km SMF transmission

As can be seen from the graphs, for BTB transmission, EVM is improved by 1.3 dB with the PDC. This happened at RF input power of -19 dBm and DC bias current of 0.5 mA. For 10 km SMF transmission, EVM is improved by 1.08 dB with the PDC. This also happened at RF input power of -19 dBm but at DC bias current of 0.4 mA. Figure 3-10 shows the measured EVMs at 5 GHz for (a) BTB transmission, and (b) 10 km SMF transmission, with and without using the PDC.

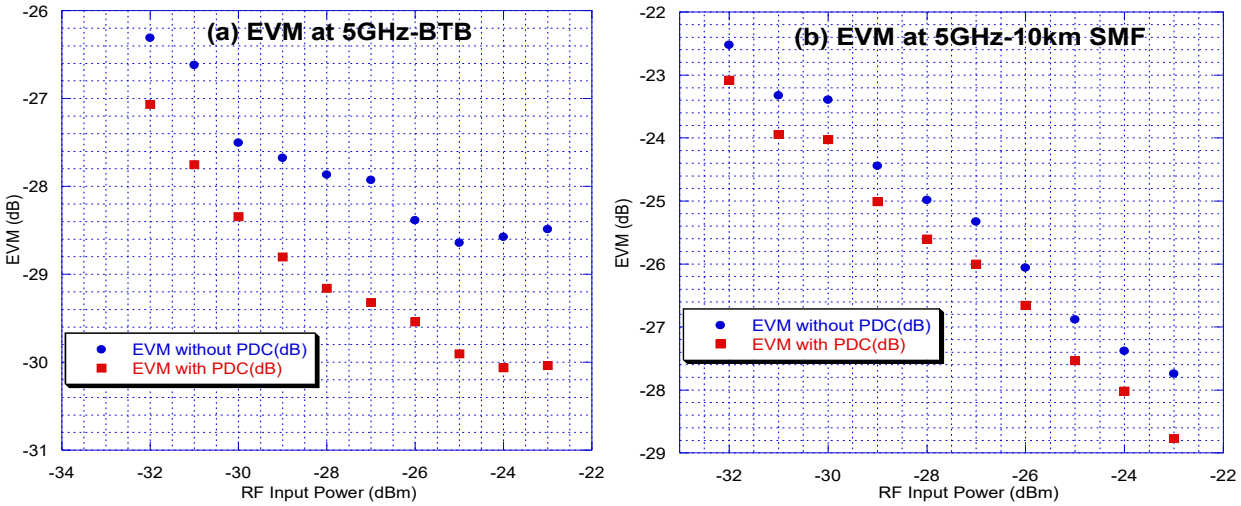

Figure 3-10: EVM at 5 GHz (a) BTB transmission, (b) 10 km SMF transmission

As can be observed from the graphs, for BTB transmission, EVM is improved by 1.55 dB with the PDC. This happened at RF input power level of -23 dBm and DC bias current of 1 mA. For 10 km SMF transmission, EVM is improved by 1.03 dB with the PDC. This also happened at RF input power level of -23 dBm but at DC bias current of 0.6 mA. The EVMs without the PDC are higher for low and high RF input powers in BTB transmission. The reason is that the noise is dominant for low RF powers and the nonlinearities are dominant for high RF powers. It can be seen that the EVM is improved by the PDC for all RF power levels and the biggest improvements happen for the high RF input power level in both BTB and 10 km SMF transmission. The EVM improvement for BTB transmission at higher RF input power level is more than the improvement for 10 km SMF transmission. Overall, EVM improvements for BTB transmission are higher compared to 10 km SMF transmission for all RF input power levels. This is because the optical fiber loss for long distance transmission induces the deterioration of signal-to-noise ratio (SNR). Due to the presence of multiple amplifiers in the experimental setup, the measurements for very high RF input powers were avoided because small increase in power of the wifi signal generated

from the AWG could unexpectedly increase the RF output power received at the DSO. Too high RF output power could burn the DSO. Therefore, use of very high RF input powers was avoided from a safety standpoint.

The investigation using wideband signals was taken a little bit further by producing Wi-Fi signals at a RF carrier of 2-5 GHz and testing for EVM improvement by using the PDC. The packet sizes for the generated signals vary at different frequencies and also the demodulation times vary at the DSO. Wifi signals at higher frequencies tend to have larger packet sizes. Figure 3-11 shows the results of EVM improvements at different frequencies for the different transmission modes. From the figure, it can be deduced that for low frequencies, the EVM improvement is bigger for both BTB and 10 km SMF transmission but becomes smaller at high frequencies. This is due to fact that more loss is induced in the system at high frequencies. The highest improvement is achieved at 2 GHz for both BTB and 10 km SMF transmission. The improvement is about 1.85 dB at 2 GHz for BTB transmission whereas for 10 km SMF transmission it is about 1.45 dB. The EVM improvement was smaller at high frequencies for 10 km SMF transmission. This is because the optical fiber loss for long distance transmission is added to the system loss at high frequencies. As can be observed from all the measurements, the EVM at different frequencies, with and without the circuit, is always less than -20 dB. It means the BER is very small and the signal transmitted is relatively error free.

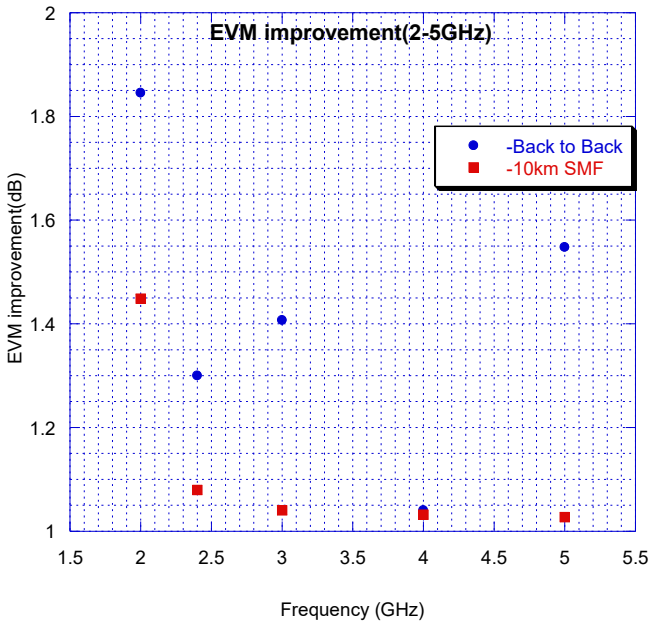

Figure 3-11: EVM improvements at different frequencies

3.3 PDC linearization for RoF transmission system using EAM OM5653C-30B

The proposed PDC was designed to simultaneously suppress the IMD3 and IMD5 non-linearities produced by the RoF transmission system using a specific EML, FLD5F20NP. However, it may not always be possible to procure the same EML at different times and for different applications because availability depends on the production life cycle by the manufacturer. Therefore, the PDC has been further tested with a different EAM. A 40 Gbit/s EAM OM5653C-30B from OKI is used for the optical subcarrier modulation in this case. The EAM has an insertion loss of 16 dB. Figure 3-12 shows (a) Photo of the EAM and (b) Transmission Characteristics of the EAM.

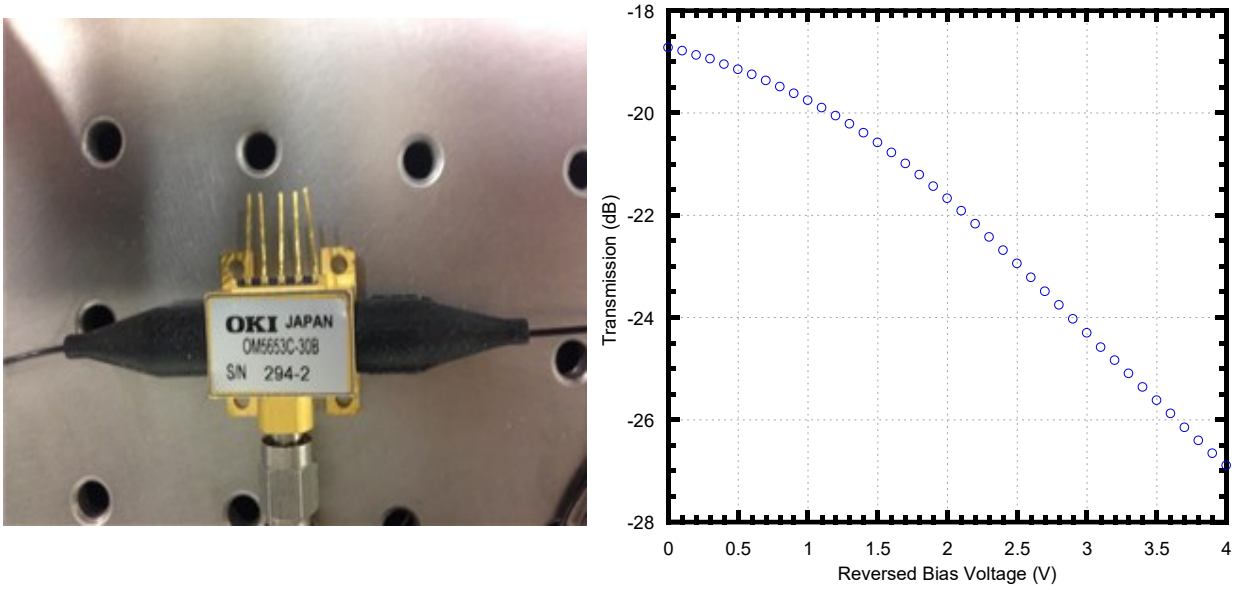

(a) (b)

Figure 3-12: (a) Photo of the EAM, and (b) Transmission characteristics of EAM OM5653C-30B

Through extensive measurements, it was determined that the EAM works best at a reversed bias voltage of 1.5 V. This is the reversed bias voltage applied for all the experiments conducted with this EAM.

Two-tone test is performed first to evaluate the PDC for linearization in the RoF transmission system using the EAM. Figure 3-13 shows the schematic of the experimental setup.

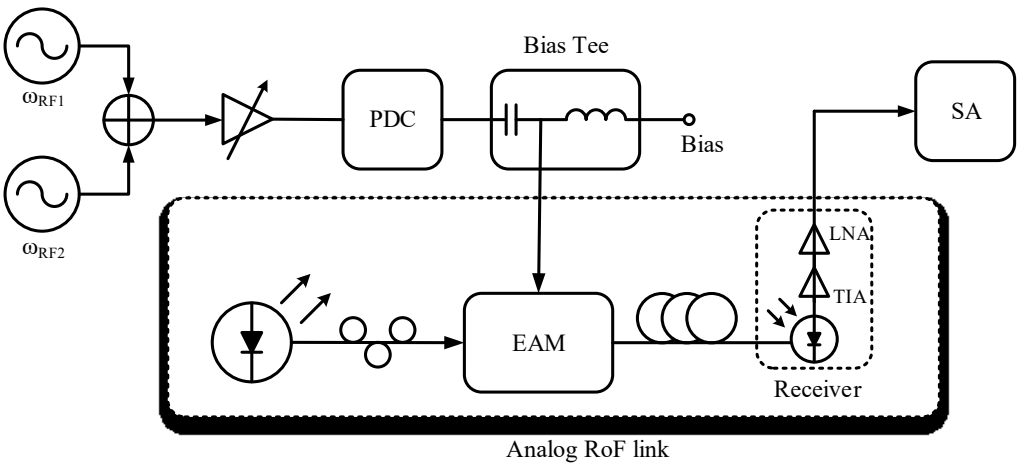

Figure 3-13: Schematic of experimental setup using EAM for two-tone test

Two RF signal generators and a broadband power combiner are used to generate a two-tone signal with a frequency spacing of 2 MHz. The signal goes through a PA ZVA-213-S+ and a variable broadband attenuator which together forms a variable PA. The PA works in its linear region. It has a gain of 26 dB and a NF of 3 dB. The PDC is connected between the variable PA and a broadband bias tee. The bias tee combines the RF signal and the reversed bias voltage for the EAM and delivers to the EAM. In the analog RoF link, the EAM is fed by an ILX Lightwave 7900B system laser source that emits CW light with optical power of 10.5 dBm at a wavelength of 1550 nm. A polarization controller (PC) is used to adjust the polarization state for the maximum output power from the EAM. The EAM is in turn connected through its optical fiber to a receiver which is a PD integrated with a TIA followed by a LNA. The receiver package is SCMR-100M6G-10-20-10 from Miteq. It converts the optical signal back to RF signal. The receiver in turn is connected to a SA U3772 from ADVANTEST where the received RF power is measured. The resolution bandwidth (RBW) of the SA is again set at 30 kHz and the video bandwidth (VBW) is set at 10 kHz. The RBW causes the RF noise floor to appear at -100 dBm during measurements. Both the RBW and VBW also affect the sweep time.

RF signals between the power levels of -15 dBm and 5 dBm at different frequencies are generated using the RF signal generators and sent through the variable PA. The combined RF signals generated at different power levels are always at frequency spacing of 2 MHz. First, the received RF powers are measured without the PDC and then they are measured with the PDC. The power levels of the received original RF signals, the IMD3s and IMD5s are measured in both

cases. When the measurements are done with the PDC connected to the setup, a DC current source is used to sweep the bias current through the diodes and the power levels are recorded when a bias current reduces the IMD3 and IMD5 components the most while minimizing the reduction in power levels of the original signals. The experiment is conducted for the entire target bandwidth of up to 6 GHz.

The best suppression for the IMD3 and IMD5 using the EAM was achieved at 2 GHz with the generated RF signals at power level of -9 dBm and bias current for the PDC circuit at 9 mA. The IMD3 was found to be suppressed by more than 2 dB and the IMD5 by ~9 dB. The SFDRs were also measured at frequencies from 1- 6 GHz and the SFDR improvement when using the PDC circuit to linearize the RoF transmission system was calculated. Figure 3-14 shows the SFDRs with and without PDC at 2 GHz.

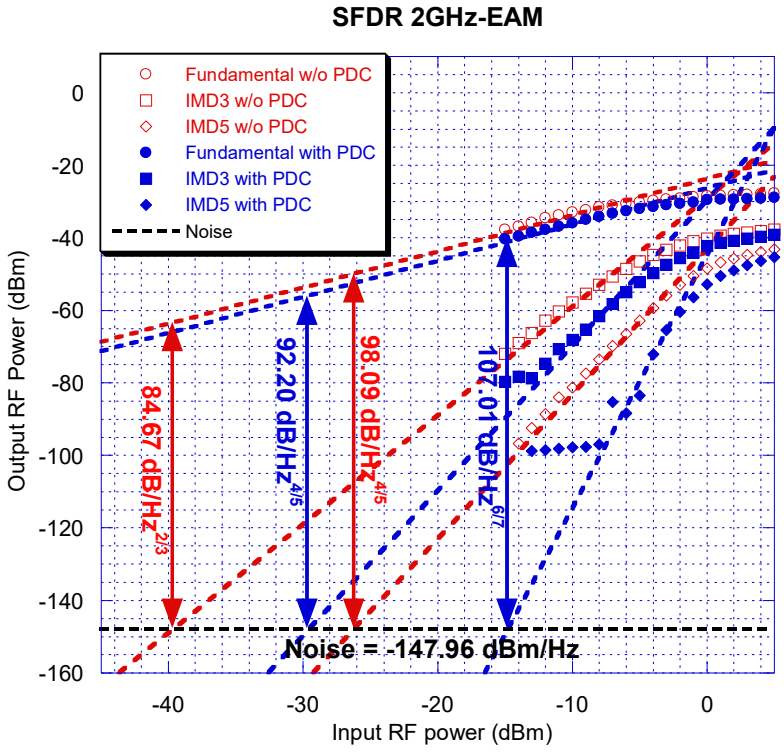

Figure 3-14: SFDR with and without PDC at 2 GHz

As can be seen from the graph, at 2 GHz, the SFDR related to IMD3 without PDC is 84.67 $dB/Hz^{2/3}$ and when the PDC circuit is added, the SFDR is 92.20 $dB/Hz^{4/5}$. That is more than 7.5 dB improvement in SFDR related to IMD3. The IMD3 is seen as 5th order limited when PDC is

used. Similarly, at 2 GHz, the SFDR related to IMD5 without the PDC is 98.09 dB/Hz$^{4/5}$ and when the PDC is used, it is 107.01 dB/Hz$^{6/7}$. That is an SFDR improvement of over 8.9 dB related to IMD5. Also, the IMD5 is 7th order limited when PDC is used. Again, reasonably best fitting lines has been used to calculate the SFDR values. As can be observed from the graph, at low RF input power, the non-linearities produced by the system with and without the PDC flats out like in previous experiments involving the EML. Suppression of non-linearities at high RF input powers when the non-linearities are significantly strong confirms the effectiveness of the PDC circuit for this case. Similarly like before, the behaviour of the non-linearities at high input power ensures that the IMD3 is 5th order limited and the IMD5 is 7th order limited when the PDC is used. Figure 3-15 shows the SFDR improvements related to (a) IMD3 and, (b) IMD5, from 1-6 GHz.

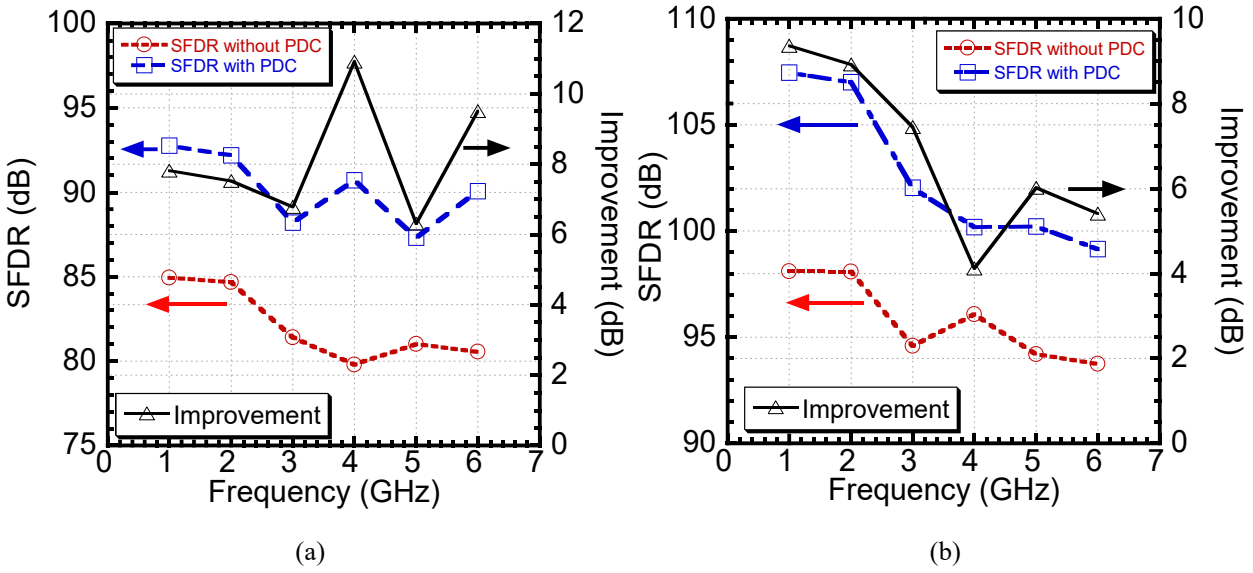

Figure 3-15: SFDR improvements related to (a) IMD3 , and (b) IMD5, from 1-6 GHz

As can be seen from the graphs, related to IMD3, the SFDR is consistently improved by over 6 dB throughout the entire target bandwidth reaching a peak of about 11 dB at 4 GHz and a low of about 6.5 dB at 5 GHz. Related to IMD5, the SFDR improvement is found to be consistently over 4 dB throughout the entire target bandwidth reaching a peak of over 9 dB at 1 GHz and a low of about 4.2 dB at 4 GHz. The fall in SFDR improvement for high frequencies can be attributed to the loss incurred by the system at high frequencies. Overall, the results show that the PDC is capable of linearizing the RoF transmission system for the entire bandwidth.

Another experiment is performed to find out if the PDC is capable of linearizing the RoF transmission system for wideband signals using this EAM. Figure 3-16 shows the photo of the setup and Figure 3-17 shows the schematic of the experimental setup. For wideband signal, Wifi signals are used at 2.4 GHz and 5 GHz and EVM improvement is measured when PDC is used for BTB transmission and 10 km SMF transmission.

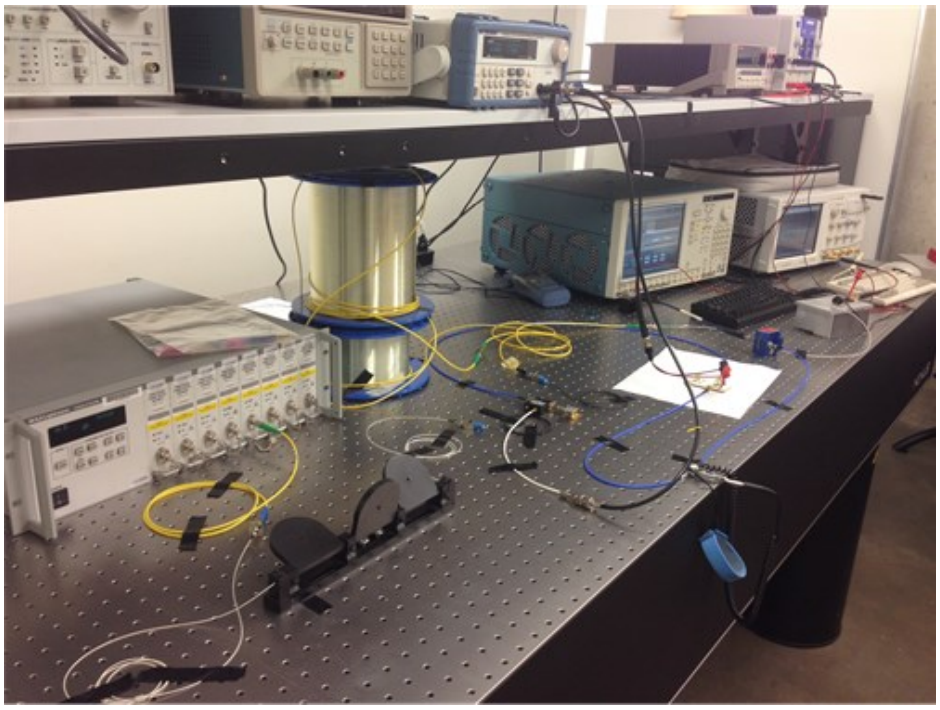

Figure 3-16: Photo of the experimental setup for EVM measurements

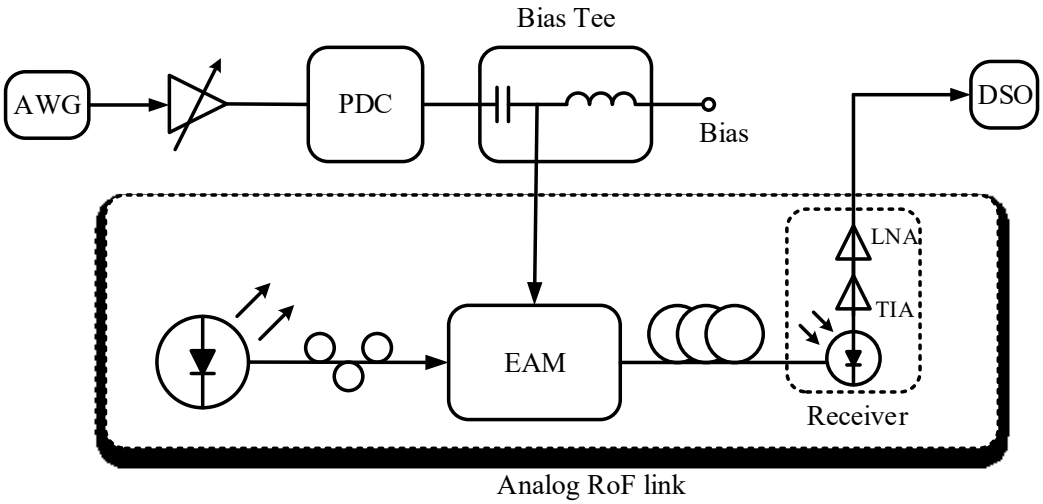

Figure 3-17: Schematic of the exerimental setup for EVM measurements

An AWG 7122B from Tektronix is used to generate Wifi signals at 2.4 GHz and 5 GHz. The generated Wifi signal goes through a PA ZVA-213-S+ and a variable broadband attenuator which together forms a variable PA. The PDC is connected between the variable PA and a broadband bias tee. The bias tee combines the generated OFDM signal and the bias voltage for the EAM and delivers to the EAM. The gain of the variable amplifier before the PDC is adjusted by 1 dB step to change the RF input power to the EAM. The RF input power is varied from -17 dBm to -8 dBm for 2.4 GHz and from –19 dBm to -10 dBm for 5 GHz. In the analog RoF link, the EAM is fed by an ILX Lightwave 7900B system laser source that emits CW light with optical power of 10.5 dBm at a wavelength of 1550 nm. A PC is used to adjust the polarization state for the maximum output power from the EAM. The EAM is in turn connected through its optical fiber to a receiver which is a PD inetgrated with TIA and LNA. A DSO 81204B from Keysight is used to receive and demodulate the Wi-Fi signals after transmission through the RoF system. For long distance transmission of the OFDM signal, a 10 km long SMF is added between the EAM and the receiver. The EVMs are measured first without using the PDC and then again by using the PDC. A DC current source is used to sweep the bias current for the diodes in the PDC and is recorded when the best EVM is achieved. Figure 3-19 shows the constellation diagrams at 2.4 GHz for (a) without PDC and (b) with PDC, for BTB transmission and (c) without PDC and (d) with PDC, for 10 km SMF transmission.

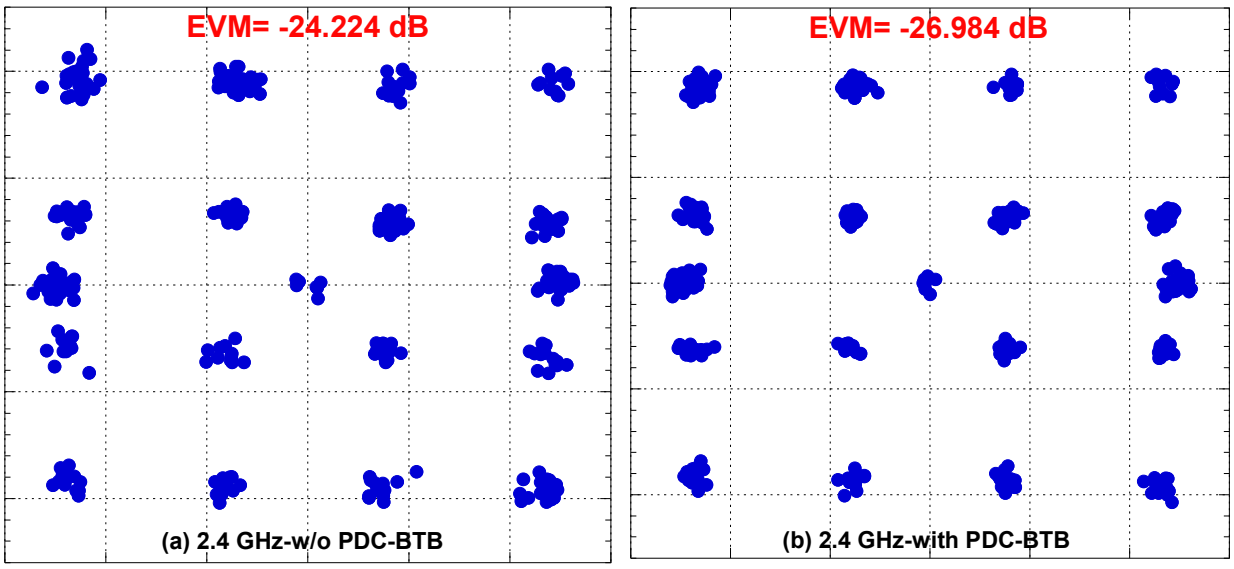

(a) (b)

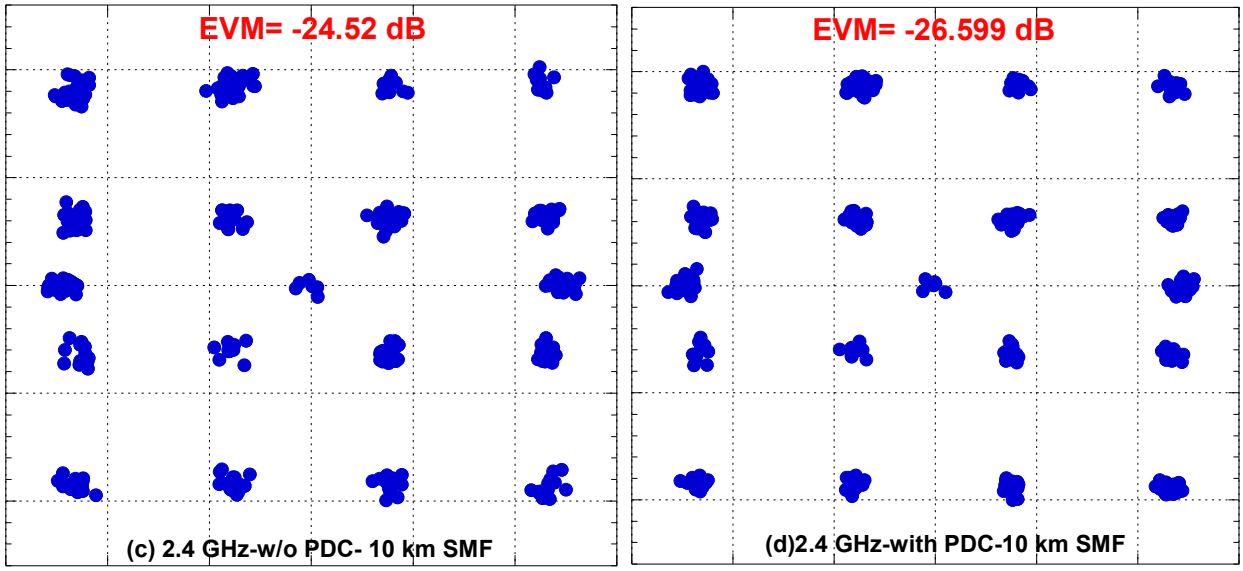

(c) (d)

Figure 3-18: EVM at 2.4 GHz (a) BTB without PDC, (b) BTW with PDC, (c) 10 km SMF without PDC, and (d) 10 km SMF with PDC

As can be observed from the constellation diagrams in Figure 3-18, the EVM improvement at 2.4 GHz for BTB transmission is 2.76 dB at RF input power level of -11 dBm and bias current of 6.9 mA. For 10 km SMF transmission, the EVM improvement is 2.08 dB at RF input power level of -11 dBm but at bias current of 6.3 mA. The low level of EVM improvement for 10 km SMF transmission can be attributed to the optical fiber loss.

Figure 3-19 (a) shows the EVM improvement at 5 GHz for BTB transmission. The EVM improves by 1.45 dB at RF input power level of -13 dBm and bias current of 3.1 mA. In Figure 3-19 (b), for 10 km SMF transmission, the EVM improves by 1.44 dB at RF input power level of -13 dBm and bias current of 3.4 mA. Compared to 2.4 GHz, the EVM imrpovements at 5 GHz are low because of system loss at high frequencies. Also, for low RF input power, lots of noise is generated at high frequencies. Therefore, the EVM improvements at low RF input power levels are also very low.

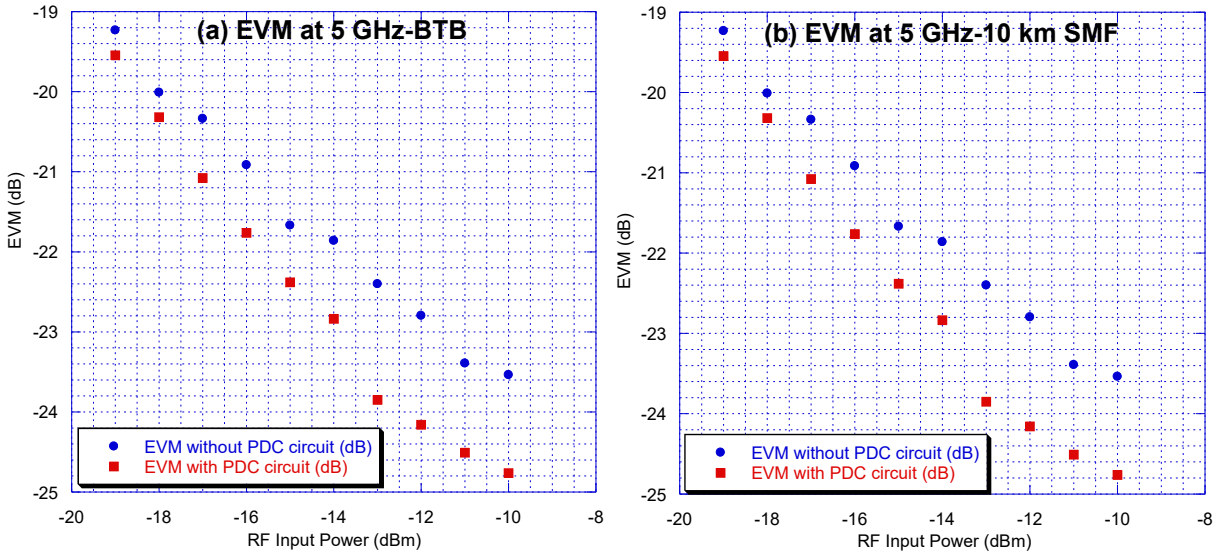

(a) (b)

Figure 3-19: EVM at 5 GHz with and without PDC for (a) BTB transmission, and (b) 10 km SMF transmission

The investigation for the wideband signal in the RoF transmission system using the EAM is continued by producing Wi-Fi signals at a RF carrier of 2-5 GHz. The EVM improvement is measured from the use of PDC for both BTB and 10 km SMF transmission modes. Figure 3-20 shows the results obtained.

As can be seen from the graph below, BTB transmission constantly produced better EVM improvements for the entire bandwidth of 2-5 GHz than 10 km SMF transmission. The highest EVM improvement of about 3.88 dB for BTB transmission happened at 3 GHz and the lowest of 1.45 dB happened at 5 GHz. For 10 km SMF transmission, highest improvement of 2.8 dB happened at 2 GHz and the lowest of 1.44 dB happened at 5 GHz. The EVM improvements are lower for 10 km SMF transmission because of optical fiber loss. The low improvement in both modes at 5 GHz is due to the high loss suffered by the PDC at high frequencies. Overall, the PDC seems to be capable of linearizing the RoF transmission system for the entire target bandwidth. The measured EVMs are again less than -20 dB in all cases. This again ensured that the BER is very low and the system is reliable and relatively error-free.

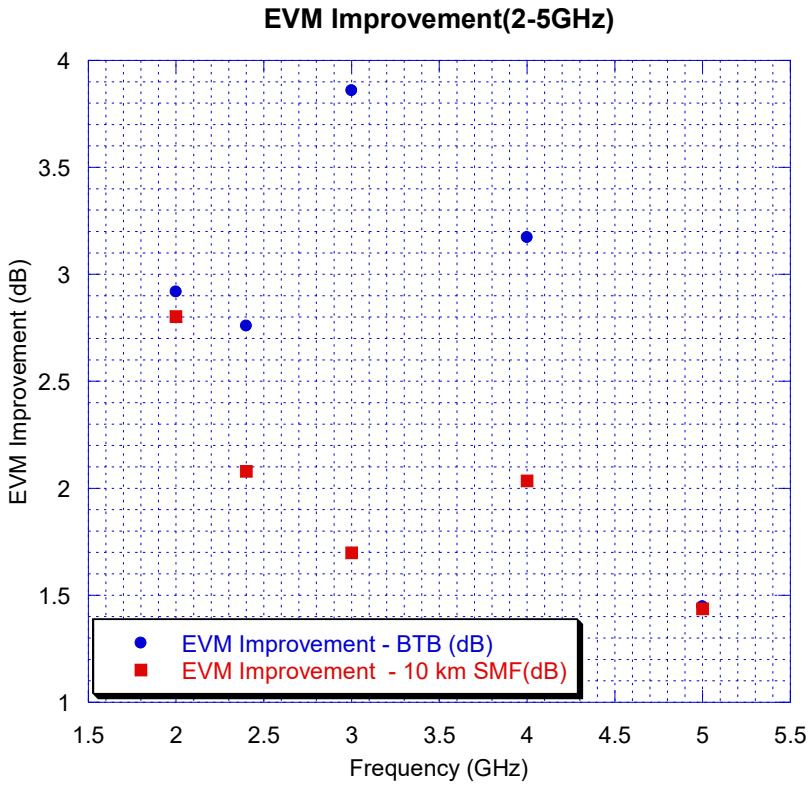

Figure 3-20: EVM improvement at different frequencies by using PDC

3.4 Summary

In this chapter, the proposed PDC circuit for simultaneous suppression of IMD3 and IMD5 in RoF transmission systems has been experimentally verified. Also, the circuit was tested for linearization of wideband signals. The experiments were done with two different setups. Firstly, the EML, FLD5F20NP, whose nonlinear characteristics was used to model the pre-distortion circuit, has been used for optical subcarrier modulation in the RoF transmission system. Two-tone test was performed first by combining two RF signal sources with a frequency spacing of 2 MHz. The circuit was tested for a bandwidth of upto 6 GHz.

The PDC suppressed IMD3 by ~6 dB and IMD5 by ~7 dB at input RF power level of -19 dBm and DC bias current of 3.5 mA at 1 GHz. SFDR was improved by more than 14 dB related to IMD3 and more than 6 dB related to IMD5. Also, the IMD3 and IMD5 with PDC were found to be 5th order and 7th order limited respectively, for high RF input power levels. Over the entire bandwidth upto 6 GHz, SFDR improvement was consistently above 11 dB related to IMD3

and above 3 dB related to IMD5. Therefore, the PDC was successful in linearizing the RoF transmission system.

The PDC was tested further by using wideband Wi-Fi signal which occupies 20 MHz bandwidth. Signals were generated at 2.4 GHz and 5 GHz and EVM improvement by using the PDC was measured for BTB and 10 km SMF transmission. For the 2.4 GHz signal, the EVM improved by 1.3 dB with PDC for BTB transmission at RF input power level of -19 dBm and DC bias current of 0.5 mA. For 10 km SMF transmission, the EVM improved by 1.08 dB with PDC at RF input power level of -19 dBm but at DC bias current of 0.4 mA. For the 5 GHz signal, the EVM improved by 1.55 dB with PDC at RF input power level of -23 dBm and DC bias current of 1 mA for BTB transmission. For 10 km SMF transmission, the EVM improved by 1.03 dB with PDC at RF input power level of -23 dBm but at DC bias current of 0.6 mA. The investigation was further extended by generating Wi-Fi signals at a RF carrier of 2-5 GHz and testing for EVM improvement using PDC. The highest improvement was achieved at 2 GHz for both BTB and 10 km SMF transmission. The improvement was about 1.85 dB for BTB transmission whereas for 10 km SMF transmission, it was about 1.45 dB. The EVM improvement was consistently above 1 dB in both modes. Measured EVMs of less than -20 dB ensured that the transmission is relatively error-free.

Next, the PDC was tested using an EAM, OMC5653C-30B, connected with a CW laser source. This investigation was done to find out if the PDC works with other modulators or not. Two-tone test was again performed first. At 2 GHz, IMD3 was found to be suppressed by more than 2 dB and IMD5 by ~9 dB. SFDR improvement was over 7.5 dB related to IMD3 and over 8.9 dB related to IMD5 at RF input power level of -9dBm and DC bias current of 9 mA. Also, IMD3 and IMD5 were again 5th order and 7th order limited when PDC is used at high RF input power levels. Over the entire bandwidth of upto 6 GHZ, related to IMD3, the SFDR was consistently improved by over 6 dB. Related to IMD5, the SFDR improvement was found to be consistently over 4 dB.

For wideband Wi-Fi signal testing, the EVM improvement at 2.4 GHz for BTB transmission was 2.76 dB at RF input power level of -11 dBm and bias current of 6.9 mA. For 10 km SMF transmission, the EVM improvement was 2.08 dB at RF input power level of -11 dBm

and bias current of 6.3 mA. The EVM improvement at 5 GHz for BTB transmission was 1.45 dB at RF input power level of -13 dBm and bias current of 3.1 mA. For 10 km SMF transmission, the EVM improved by 1.44 dB at RF input power level of -13 dBm and bias current of 3.4 mA. For Wi-Fi signals at a RF carrier of 2-5 GHz, the EVM improvement was consistently above 1.45 dB for BTB transmission and above 1.44 dB for 10 km SMF transmission. Again, measured EVMs of less than -20 dB ensured the relatively error-free nature of the transmission.

Overall, the PDC circuit seemed to confirm its ability to suppress IMD3 and IMD5 simultaneously and to linearize wideband signals in RoF transmission systems. It also showed its ability to work with different modulators used for optical subcarrier modulation in RoF transmission systems.

Chapter 4 Conclusion

4.1 Concluding Remarks

Radio-over-fiber transmission system is a hot research topic right now because of the urgent need to provide reliable wireless access networks for the ever increasing need of connectivity in our smartphone and tablet dominated world. RoF transmission system has transparent infrastructure and can support various wireless access technologies. However, it is susceptible to nonlinearities. Optical subcarrier modulation is the main nonlinear source in RoF transmission systems. Research focus has been mainly on the removal of IMD3 because it has the highest power of all the odd order nonlinearities. It is situated very close to fundamental RF signals and cannot be filtered out because it falls in the passband of the transmission system. IMD5 has the next highest power among odd order nonlinearities and also fall in the passband. Because of its low power, it doesn't receive as much attention as IMD3 but nevertheless IMD5 can also degrade transmission to some extent. Therefore, both IMD3 and IMD5 need to be suppressed.

In this thesis, the focus has been placed on designing an analog PDC that can suppress both IMD3 and IMD5 simultaneously for bandwidth up to 6 GHz. Also, it was needed to linearize wideband signals in RoF transmission systems. Therefore, an analog PDC was designed using two beam-lead schottky diodes in anti-parallel combination as predistorter. The diode combination formed a push-pull structure which made sure to produce only odd order nonlinearities for pre-distortion and eliminated all the even order nonlinearities. The objective was to produce a low cost and low power consuming device.

Experiments were conducted in two different environments using two-tone RF signals and wideband Wi-Fi signals at 2.4 GHz and 5 GHz:

1. First the EML, FLD5F20NP, that was used to model the circuit for pre-distortion was used to perform optical subcarrier modulation in RoF system. Two-tone tests showed suppression of IMD3 by ~6 dB and IMD5 by ~7 dB at 1 GHz. SFDR was improved by more than 14 dB related to IMD3 and more than 6 dB related to IMD5. SFDR improvement was consistently above 11 dB related to IMD3 and above 3 dB

related to IMD5 for entire target bandwidth. The IMD3 and IMD5 with PDC were found to be 5^{th} order and 7^{th} order limited for high RF input powers. Tests with wideband Wi-Fi signals at 2.4 GHz and 5 GHz were also performed and EVM improvement by using the PDC was measured for BTB and 10 km SMF transmission modes. For the 2.4 GHz signal, the EVM was improved by 1.3 dB with PDC for BTB transmission. For 10 km SMF transmission, the EVM was improved by 1.08 dB with PDC. For the 5 GHz signal, the EVM was improved by 1.55 dB with PDC for BTB transmission. For 10 km SMF transmission, the EVM was improved by 1.03 dB with PDC. Upon further investigation with Wi-Fi signals at a RF carrier of 2-5 GHz, the highest improvement was achieved at 2 GHz for both BTB and 10 km SMF transmission. The improvement was about 1.85 dB for BTB transmission whereas for 10 km SMF transmission it was about 1.45 dB. The EVM improvement was consistently above 1 dB in both modes. Measured EVM of less than -20 dB ensured that BER is low for the transmission and therefore, relatively error-free.

2. Next, the PDC was tested using an EAM, OMC5653C-30B, connected with a CW laser source. Two-tone tests showed that, at 2 GHz, IMD3 was suppressed by more than 2 dB and IMD5 by ~9 dB. SFDR improvement was over 7.5 dB related to IMD3 and over 8.9 dB related to IMD5. Over the entire bandwidth of upto 6 GHZ, related to IMD3, the SFDR was consistently improved by more than 6 dB. Related to IMD5, the SFDR improvement was found to be consistently over 4 dB. Again, the IMD3 and IMD5 with PDC were found to be 5^{th} order and 7^{th} order limited at high RF input power levels. For wideband Wi-Fi signal testing, the EVM improvement at 2.4 GHz for BTB transmission was 2.76 dB. For 10 km SMF transmission, the EVM improvement was 2.08 dB. The EVM improvement at 5 GHz for BTB transmission was 1.45 dB. For 10 km SMF transmission, the EVM improved by 1.44 dB. For Wi-Fi signals at a RF carier of 2-5 GHz, the EVM improvement was consistently above 1.45 dB for BTB transmission and above 1.44 dB for 10 km SMF transmission. Like in previous case, the measured EVMs were

again less than -20 dB. Therefore, transmission was relatively error free due to very low BER.

The PDC circuit seemed to fulfill the objectives of suppressing IMD3 and IMD5 simultaneously. For wideband signals, it also linearized the transmission. Even though the power consumption was high in the second scenario than the first, the overall power consumption was still relatively low considering the fact that the required DC bias current for the diodes was less than 10 mA in both cases.

4.2 Future Work

One of the future studies about the linearization technologies will focus on the simultaneous suppressions of several nonlinearities while at the same time reducing the memory effect. Digital linearization can reduce memory effect but suffers from low bandwidth. Therefore, a hybrid approach of using analog PDC coupled with digital filters for broadband linearization and reduction of memory effect may be of interest.

Also, another enhancement would be to tune the proposed PDC to work for even lower bias current thus making it even less power consuming.

It would be also useful to find a way to mitigate for the high loss at high frequencies thus making it useful for simultaneous IMD3 and IMD5 suppression for ultra broadband transmission.

Reference

[1] A.J.Cooper, 'Fiber/radio for the provision of cordless mobile telephony services in the access network', *Electronics letters*, vol. 26 no. 24, pp. 2054 – 2056, Nov.1990.

[2] Xiupu Zhang, Ran Zhu, Dongyan Shen, Taijun Liu, 'Linearization technologies for broadband Radio-over-Fiber transmission systems', *Photonics,* vol.1, no. 4, pp. 455-472, Nov. 2014.

[3] Arun Joseph, Shanthi Prince, 'Performance analysis and optimization of radio over fiber link', *International Conference on Communications and Signal Processing (ICCSP)*, pp. 1599 – 1604, Apr. 2014.

[4] U. Sampath Kumar, V. Saminadan and P. Williams, 'Performance evaluation of millimeter wave and UWB signals over fiber radio networks', *International Conference on Communications and Signal Processing (ICCSP)*, pp. 104 – 107, Apr. 2012.

[5] J. Park, W. V. Sorin, and K. Y. Lau, "Elimination of the fiber chromatic dispersion penalty on 1550 nm millimeter-wave optical transmission," *Electron. Lett.*, vol. 33, issue 6, pp. 512-513, Mar. 1997.

[6] G. H. Smith, D. Novak, and Z. Ahmed, "Overcoming chromatic-dispersion effects in fiber-wireless systems incorporating external modulators," *IEEE Trans. Microw. Theory Techn.*, vol. 45, issue 8, pp. 1410–1415, Aug. 1997.

[7] G. H. Smith, D. Novak, and Z. Ahmed, "Technique for optical SSB generation to overcome dispersion penalties in fiber-radio systems," *Electron. Lett.* vol. 33, no. 1, pp. 74-75, Jan. 1997.

[8] A. Bjarklev, T. Rasmussen, O. Lumholt, K. Rottwitt, and M. Helmer, "Optimal design of single-cladded dispersion-compensating optical fibers," *Opt. Lett.*, vol. 19, issue 7, pp. 457–459, Apr. 1994.

[9] A. J. Antos and D. K. Smith, "Design and characterization of dispersion compensating fiber based on the LP01 mode," *J. Lightw. Technol.*, vol. 12, issue 10, pp. 1739–1745, Oct. 1994.

[10] David M. Pozar, *Microwave Engineering*, 3rd ed., 2005, John Wiley & sons, Inc.

[11] B. Masella, B. Hraimel, and X. Zhang, "Enhanced spurious-free dynamic range using mixed polarization in optical single sideband Mach-Zehnder modulator," *J. Lightw. Technol.*, vol. 27, no. 15, pp. 3034–3041, Aug. 2009.

[12] B. Hraimel, X. Zhang, W. Jiang, K. Wu, T. Liu, T. Xu, Q. Nie, and K. Xu, "Experimental demonstration of mixed-polarization to linearize electro-absorption modulators in radio-over-fiber links," *IEEE Photon. Technol. Lett.*, vol. 23, no. 4, pp. 230-232, Feb. 2011.

[13] B. Hraimel and X. Zhang, "Performance improvement of radio-over fiber links using mixed-polarization electro-absorption modulators," *IEEE Trans. Microw. Theory Techn.*, vol. 59, issue 12, pp. 3239–3248, Dec. 2011.

[14] B. Hraimel and X. Zhang, "Characterization and compensation of AM-AM and AM-PM distortion in mixed polarization radio over fiber systems," *IEEE MTT-S Int. Microw. Symp. Dig.*, Jun. 2012.

[15] B. Hraimel, X. Zhang, T. Liu, T. Xu, Q. Nie, and D. Shen, "Performance enhancement of an OFDM ultra-wideband transmission-over-fiber link using a linearized mixed-polarization single-drive x-cut Mach-Zehnder modulator," *IEEE Trans. Microw. Theory Techn.*, vol. 60, issue 10, pp. 3328–3338, Oct. 2012.

[16] D. J. M. Sabido, IX, M. Tabara, T. K. Fong, C. L. Lu, and L. G. Kazovsky, "Improving the dynamic range of a coherent am analog optical link using a cascaded linearized modulator," *IEEE Photon. Technol. Lett.*, vol. 7, no. 7, pp. 813-815, Jul. 1995.

[17] J. Li et al., "Third-order intermodulation distortion elimination of microwave photonics link based on integrated dual drive dual-parallel Mach–Zehnder modulator," Opt. Exp., vol. 38, no. 21, pp. 4285–4287, Nov. 2013.

[18] H. Zhang, S. Pan, M. Huang, and X. Chen, "Linear analog photonic link based on cascaded polarization modulators," *Asia Commun. Photon. Conf.*, Nov. 2012.

[19] Y. Cui, K. Xu, J. Dai, X. Sun, Y. Dai, Y. Ji, and J. Lin, "Overcoming chromatic-dispersion-induced power fading in RoF links employing parallel modulators," *IEEE Photon. Technol. Lett.*, vol. 24, no. 14, pp. 1173-1175, Apr. 2012.

[20] K. K. Loi, J. H. Hodiak, X. B. Mei, C. W. Tu, and W. S. C. Chang, "Linearization of 1.3-μm MQW electro absorption modulators using an all-optical frequency-insensitive technique," *IEEE Photon. Technol. Lett.*, vol. 10, no. 7, pp. 964-966, Jul. 1998.

[21] B. M. Hass, V. J. Urick, J. D. McKinney, and T. E. Murphy, "Dual-wavelength linearization of optical-modulated analog microwave signals," *J. Lightw. Technol.*, vol. 26, no. 15, pp. 2748–2753, Aug. 2008.

[22] Z. Wu, K. Xu, J. Niu, Q. Lv, Y. Dai, and J. Lin, "Third-order intermodulation distortion improvement radio-over-fiber link using dual-wavelength intensity modulation," *High Speed Intell. Commun. Forum*, May 2012.

[23] Ran Zhu, Xiupu Zhang 'Linearization of radio-over-fiber systems by using two lasers with different wavelengths', *International Microwave Symposium (IMS), IEEE MTT-S,* pp. 1-3, Jun. 2014.

[24] L. C. Vieira, N. J. Gomes, and A. Nkansah, "An experimental study on digital predistortion for radio-over-fiber links," *Asia Commun. Photon. Conf. Exhibition*, pp. 126-127, Dec. 2010.

[25] Z. Xuan, "Digital Predistortion for Broadband Radio-over-Fiber Transmission Systems," Master's Thesis, Concordia University, Nov. 2015.

[26] C. H. Lee, V. Postoyalko, and T. O'Farrell, "Enhanced performance of RoF link for cellular mobile systems using postdistortion compensation," *IEEE Int. Symp. Pers. Indoor Mobile Radio Commun*, pp. 2772-2776, Sept. 2004.

[27] Yiming Shen, Bouchaib Hraimel, Xiupu Zhang, Glenn E. R. Cowan, Ke Wu, Taijun Liu, 'A novel analog broadband RF predistortion circuit to linearize electro-absorption modulators

in multiband OFDM Radio-over-Fiber systems', *IEEE Transactions on Microwave Theory and Techniques*, vol. 58, no. 11, pp. 3327 – 3335, Nov. 2010.

[28] Ran Zhu, Zichen Xuan, Ye Zhang, Xiupu Zhang and Dongya Shen, 'Novel broadband analog predistortion circuit for radio-over-fiber systems', *IEEE MTT-S International Microwave Symposium (IMS), 2015*, pp. 1-4, May 2015.

[29] Matsubara H., Ishihara K., Miyadai N., Nojima T.: 'Simultaneous 3rd-and-5th-order intermodulation compensation with cuber predistortion and 2nd harmonics injection for microwave power amplifiers'. Proc. 6th Int. Kharkov Symp. Physics and Engineering of Microwaves Millimeter and Submillimeter Waves and Workshop on Terahertz Technologies, Kharkov, Ukraine, June 2007, pp. 532–534

[30] Tae-Kyeong Lee ; Yon-Tae Moon ; Hong-Seung Kim and Young-Wan Choi: "Cancellation of the IMD3 and IMD5 using opto-electrical predistortion optical transmitter for radio-over-fiber systems", Proc. SPIE 7620, Broadband Access Communication Technologies IV, 76200A (January 22, 2010);

[31] Tae-Kyeong Lee, Yon-Tae Moon, Hong-Seung Kim, Young-Wan Choi, "Theoretical analysis and realization of opto-electrical predistortion optical transmitter for the simultaneous suppression of IM3 and IM5 signal," Optics Communications, Volume 285, Issues 10–11, 15 May 2012, Pages 2697-2701, ISSN 0030-4018

[32] Avago HSCH-5314 Datasheet, Avago Technologies, [Online] available http://www.avagotech.com/docs/AV01-0484EN.

[33] R. A. Shafik, S. Rahman, and R. Islam, "On the extended relationships among EVM, BER and SNR as performance metrics," in Proc. IEEE ICECE, Dec. 2006, pp. 408–411.

[34] Y. Shen, "A Novel Analog Broadband RF Predistortion Circuit to Linearize Electro-absorption Modulators in Multiband OFDM Ultra-Wideband Radio over Fiber Systems," Master's Thesis, Concordia University, Apr. 2010.